Using an independent geochronology based on palaeomagnetic secular variation (PSV) and atmospheric Pb deposition to date Baltic Sea sediments and infer 14C reservoir age

Lougheed, Bryan C.; Snowball, Ian; Moros, Matthias; Kabel, Karoline; Muscheler, Raimund; Virtasalo, Joonas J.; Wacker, Lukas

Published in:
Quaternary Science Reviews

DOI:
10.1016/j.quascirev.2012.03.013

2012

Document Version:
Publisher's PDF, also known as Version of record

Using an independent geochronology based on palaeomagnetic secular variation (PSV) and atmospheric Pb deposition to date Baltic Sea sediments and infer ^{14}C reservoir age.

B.C. Lougheed[a,], I. Snowball[a], M. Moros[b], K. Kabel[b], R. Muscheler[a], J. J. Virtasalo[c], L. Wacker[d]

[a] *Department of Geology, Lund University, Sölvegatan 12, 22362 Lund, Sweden.*
[b] *Leibniz Institute for Baltic Sea Research, Seestraße 15, 18119 Rostock-Warnemünde, Germany.*
[c] *Geological Survey of Finland, P.O. Box 96, 02151 Espoo, Finland.*
[d] *Institute for Particle Physics, ETH Zürich, 8093 Zürich, Switzerland.*

Abstract

Dating of sediment cores from the Baltic Sea has proven to be difficult due to uncertainties surrounding the ^{14}C reservoir age and a scarcity of macrofossils suitable for dating. Here we present the results of multiple dating methods carried out on cores in the Gotland Deep area of the Baltic Sea. Particular emphasis is placed on the Littorina stage (8 ka ago to the present) of the Baltic Sea and possible changes in the ^{14}C reservoir age of our dated samples. Three geochronological methods are used. Firstly, palaeomagnetic secular variations (PSV) are reconstructed, whereby ages are transferred to PSV features through comparison with varved lake sediment based PSV records. Secondly, lead (Pb) content and stable isotope analysis are used to identify past peaks in anthropogenic atmospheric Pb pollution. Lastly, ^{14}C determinations were carried out on benthic foraminifera (*Elphidium spec.*) samples from the brackish Littorina stage of the Baltic Sea. Determinations carried out on smaller samples (as low as 4 µg C) employed an experimental, state-of-the-art method involving the direct measurement of CO_2 from samples by a gas ion source without the need for a graphitisation step - the first time this method has been performed on foraminifera in an applied study. The PSV chronology, based on the uppermost Littorina stage sediments, produced ten age constraints between 6.29 and 1.29 cal ka BP, and the Pb depositional analysis produced two age constraints associated with the Medieval pollution peak. Analysis of PSV data shows that adequate directional data can be derived from both the present Littorina saline phase muds and Baltic Ice Lake stage varved glacial sediments. Ferrimagnetic iron sulphides, most likely authigenic greigite (Fe_3S_4), present in the intermediate Ancylus Lake freshwater stage sediments acquire a gyroremanent magnetisation during static alternating field (AF) demagnetisation, preventing the identification of a primary natural remanent magnetisation for these sediments. An inferred marine reservoir age offset (ΔR) is calculated by comparing the foraminifera ^{14}C determinations to a PSV & Pb age model. This ΔR is found to trend towards younger values upwards in the core, possibly due to a gradual change in hydrographic conditions brought about by a reduction in marine water exchange from the open sea due to continued isostatic rebound.

1. Introduction

The Baltic Sea underwent significant developments since the last deglaciation, involving alternating fresh and saline stages. The earliest stage, which ceased some 10 ka ago, is known as the Baltic Ice Lake, an ice dammed freshwater lake. The ice dam was eventually breached at Mt. Billingen (58.5°N, 13.8°E) and the Baltic Ice Lake drained down to equilibrium with eustatic sea level through a pathway across the Swedish mainland, initiating the saline Yoldia Sea stage (from 10 ka ago to 9.5 ka ago). Due to isostatic rebound, the Baltic Sea basin eventually became once more isolated from eustatic sea level, leading to the development of the freshwater Ancylus Lake stage (from 9.5 ka ago to 8.0 ka ago). A connection with the open sea was achieved once more when eustatic sea level rose above the Drogden and Darss sills (Figure 1) approximately 8.0 ka ago, initiating the current saline Littorina Sea stage. Continued uplift of the Baltic Sea basin throughout Littorina stage has led to reduced exchange with the open sea across the sills. A more detailed account of the evolution of the described stages can be found in Björck (1995).

The current, Littorina stage of the Baltic Sea development is that of a semi-enclosed basin whereby open exchange of saline water with the Kattegat and Skagerrak is severely limited by the presence of the Drogden and Darss sills (Figure 1). Inflow of deeper saline water is overlain by freshwater discharge from the Baltic catchment, leading to the formation of a permanent halocline in the Baltic Sea. This estuarine-like circulation system, combined with the relatively

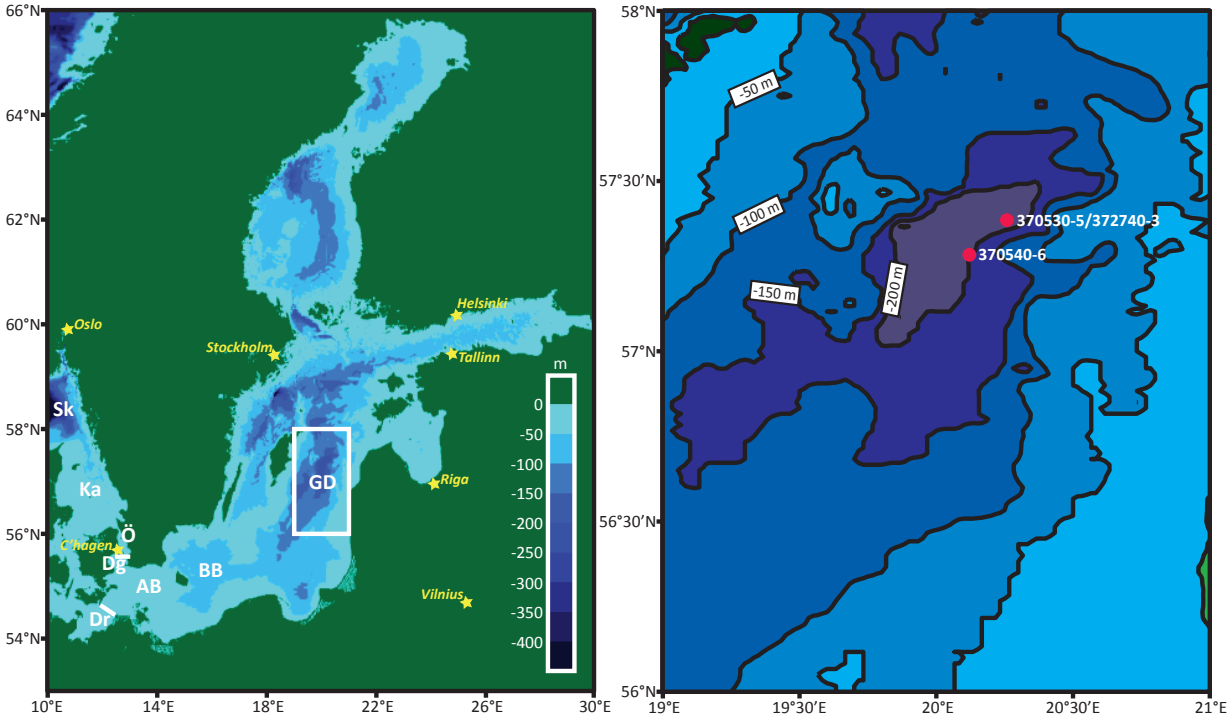

Fig. 1. Left: overview of Baltic Sea bathymetry including Gotland Deep study area (white box). Baltic Sea features abbreviated as follows; Skagerrak (Śk), Kattegat (Ka), Öresund (Ö). Drogden Sill (Dg), Darss Sill (Dr), Arkona Basin (AB), Bornholm Basin (BB), Gotland Deep (GD). Right: Bathymetry of Gotland Deep study area including coring locations. Bathymetric data from IOC et al. (2003).

isolated nature of the sea, has made radiocarbon dating of organic fossil taxa difficult, due to the subsequent uncertainties surrounding the ^{14}C reservoir age. This reservoir age can vary both spatially and temporally. A study area's proximity to sources of freshwater discharge or saline inflow can influence its ^{14}C reservoir age, as both sources input endemic carbon into the estuarine-like system. Additionally, the Baltic Sea has changed significantly in extent even throughout the Littorina stage, having been subjected to both eustatic sea level change and isostatic rebound, which persists today. The change in relative sea level has influenced the rate of exchange of seawater across the Drogden and Darss sills, while changes in river runoff have altered the fluxes of particulate and dissolved carbon from the catchment area. These processes could have affected the ^{14}C reservoir age in the Baltic Sea through time. Additionally, a scarcity of macrofossils in the Baltic Sea has meant that bulk sediment dates have often been used for ^{14}C chronologies, but these can often be influenced by older, reworked carbon. Rößler et al. (2011) show that, in the case of the Arkona Basin, bulk ^{14}C determinations can be up to 1,000 ^{14}C years older than ^{14}C determinations based on foraminifera from the same stratigraphic level. Similar issues with bulk dating have been noted in other studies (e.g. Hedenström and Possnert, 2001).

The difficulties surrounding ^{14}C dating in the Baltic Sea have led, in recent years, to researchers pursuing other geochronological methods to complement ^{14}C dating for mid to late Holocene Baltic Sea sediments. Kotilainen et al. (2000) applied palaeomagnetic methods to determine the palaeomagnetic secular variation (PSV) in a Gotland Deep sediment core and the PSV data were then compared to those from a Finnish lake with ages based on a varve chronology. The transferred varved ages generally agreed with ^{14}C dates carried out on bulk sediment, driftwood and shells in the Gotland Deep core. Declination data were less clear, however, and the declination swing associated with one of the main Holocene PSV features in the region, easterly declination maximum '*f*' (Turner and Thompson, 1981; Snowball et al., 2007), was not readily discernable. Optically stimulated luminescence (OSL) dating of Baltic Sea sediments from the Arkona Basin was carried out by Kortekaas et al. (2007). OSL dating was found to be suitable in this basin, although the date of a major lithographical transition (Ancylus-Littorina) conflicted with the previously established date (e.g. Björck, 1995). Bindler et al. (2009) has identified Pb peaks in sediments from the Gotland Deep region, but these were not used to construct isochrones. Recently, however, Zillén et al. (2012) successfully used Pb deposition history to construct isochrones in the Baltic Sea proper, based on

the Pb deposition peaks associated with 20th century, Medieval and Roman periods.

Previous Baltic Sea basin chronologies have been based on ^{14}C dating of bulk material. For the first time, we present ^{14}C determinations on foraminifera for Littorina stage sediments in the central basin (Gotland Deep). We also present an independent geochronology based on PSV and Pb deposition age constraints, also covering Littorina stage sediments. Our independent geochronology allows us to use the aforementioned ^{14}C determinations to investigate radiocarbon reservoir age variations in this basin.

2. Hydrographic setting

In this study we concentrate mostly on the Littorina stage evolution of the Gotland Deep area of the Baltic Sea. The Gotland Deep is one of the deepest areas of the Baltic Sea proper (Figure 1) and has been underneath the Baltic Sea halocline since observational records began (SMHI, 2011). The strong stratification of the sea in this area means that the Gotland Deep area is prone to hypoxic conditions and laminated sediments are widespread throughout (e.g. Winterhalter et al., 1981; Sohlenius et al., 2001; Conley et al., 2002; Zillén et al., 2008). Laminated sections are interrupted by intervals of intensely bioturbated sediment, which records time intervals of oxygenation and macrofaunal occupation of the seafloor (Virtasalo et al., 2011b). The Gotland Deep is influenced by inflowing saline water which, due to its greater density, seeks deeper areas of the sea. However, this water is entrained by brackish outflowing water and is reduced, by more than half, in salinity on its journey from the open sea at the Skaggerak to the Gotland Deep. The marine environment in the Gotland Deep is, therefore, that of saline inflow that has undergone significant mixing with the brackish outflowing water and this should be reflected in the ^{14}C reservoir age.

As the cores were taken from a depocentre, the sediment accumulation rate is quite high, leading to a higher resolution recording of PSV than would be available in shallower areas. Acoustic profiles recorded for the location of sediment cores 370530-5 and 372740-3 suggest that the reflector associated with the top of the Ancylus clays is situated at approximately 6 m sediment depth. The depth of the same reflector for sediment core 370540-6 was at 4 m. The chosen coring locations have sediment that accumulates in horizontal layers with minimum discontinuities present, which is useful for PSV analysis.

3. Method

3.1 Core retrieval and subsampling

The three cores, 370530-5, 370540-6 and 372740-3, were retrieved (Table 1 and Figure 1) on board R/V Aranda (April 2009) and R/V Maria S. Merian (September 2009). Sediment core 372740-3 was taken to complement core 370530-5 and was therefore retrieved from the same location.

The sediment cores were retrieved in plastic liners, using a nine or six metre gravity corer with a 12 cm diameter steel barrel. The liners were marked with a line before coring to ensure consistent orientation between sections, seeing as the liners were cut into one metre sections as they were extruded from the core barrel. It is thought that approximately the top 30 cm of sediment is lost as a consequence of the gravity coring process. Comparison with loss-on-ignition (LOI) data from short cores taken at the same sites confirmed this. On-board discrete subsampling for palaeomagnetism was carried out on cores 370530-5 and 370540-6 after opening, splitting and photographing of the core sections. The discrete subsampling was carried out at a 3 cm resolution using standard plastic palaeomagnetic sample boxes with an internal volume of 7 cm^3. All samples were wrapped in plastic film and stored in a controlled humidity environment at 4°C to limit chemical alteration of the samples. Core 370530-5 was additionally subsampled for fabric analysis using elongated plastic channels of 50x5x2 cm in dimension.

3.2 Loss-on-Ignition (LOI)

All three cores were analysed for weight LOI at a one centimetre resolution at IOW. These measurements were carried out on the original core material and not the discrete cube subsamples. LOI was determined by ashing freeze-dried samples at 550 °C for three hours and calculating the resulting mass difference.

Table 1. Cores retrieved for study.

Core	Latitude	Longitude	Depth (m)	Length (m)	Cruise	Equipment
370530-5	57°23.12'N	20°15.49'E	231	4.98	R/V Aranda, Apr. 2009	6 m gravity corer
372740-3	57°23.10'N	20°15.50'E	232	7.64	R/V Maria S. Merian , Sep. 2009	9 m gravity corer
370540-6	57°17.01'N	20°07.25'E	243	7.43	R/V Aranda, Apr. 2009	9 m gravity corer

3.3 Fabric Analysis

Sedimentological and ichnological characteristics of the sediments were studied using X-radiographs and digital images of core 370530-5. The subsampled 50x5x2 cm channels were imaged using a custom made tungsten-anode micro-computed tomography Nanotom device supplied by Phoenix | Xray Systems + Services GmbH at the Laboratory of Microtomography, University of Helsinki (for details, see Virtasalo et al., 2011a). The sediments were classified into thinly laminated, bio-deformed and burrow-mottled sedimentary fabrics following Virtasalo et al. (2011b). The thinly laminated sedimentary fabric records periods of seafloor anoxia with an absence of macrofauna, whereas the bio-deformed fabric records brief periods with low oxygen levels that punctuate the anoxic background conditions, thereby permitting colonisation by pioneering nectobenthos-dominated fauna, which scrape the sediment surface through poorly specialised feeding and resting activities. The burrow-mottled fabric records longer lasting oxic conditions, when endobenthic macrofauna occupy the surface sediments and produce burrow structures, which are preserved in the sediment column.

Table 2. Sediment units incores retrieved for study

Sediment core 370530-5		
Unit	Depth interval (cm)	Sedimentological description
1	0 - 98	Strongly laminated dark black/grey clay gyttja with high water content.
2	98 - 158	Alternating strongly laminated dark black/grey clay gyttja and faintly laminated grey clay gyttja.
3	158 - 300	Faintly laminated/burrow-mottled grey clay gyttja.
4	300 - 448	Strongly laminated dark black/grey clay gyttja.
5	448 - 465	Faintly laminated/burrow-mottled grey clay gyttja.
6	465 - core bottom	Strongly laminated dark black/grey clay gyttja.
Sediment core 372740-3		
Unit	Depth interval (cm)	Sedimentological description
1	0 - 106	Strongly laminated dark black/grey clay gyttja with high water content.
2	106 - 156	Alternating strongly laminated dark black/grey clay gyttja and faintly laminated grey clay gyttja.
3	156 - 287	Faintly laminated/burrow-mottled grey clay gyttja.
4	287 - 449	Strongly laminated dark black/grey clay gyttja.
5	449 - 472	Faintly laminated/burrow-mottled grey clay gyttja.
6	472 - 556	Strongly laminated dark black/grey clay gyttja.
7	566 - 599	Faintly laminated/burrow-mottled grey clay gyttja.
8	599 - 656	Bluish-grey clay with dark banding that oxidises to orange/red.
Sediment core 370540-6		
Unit	Depth interval (cm)	Sedimentological description
1	0 - 94	Strongly laminated dark black/grey clay gyttja with high water content.
2	94 - 122	Alternating strongly laminated dark black/grey clay gyttja and faintly laminated grey clay gyttja.
3	122 - 202	Faintly laminated/burrow-mottled grey clay gyttja.
4	202 - 321	Strongly laminated dark black/grey clay gyttja.
5	321 - 339	Faintly laminated/burrow-mottled grey clay gyttja.
6	339 - 390	Strongly laminated dark black/grey clay gyttja.
7	390 - 416	Faintly laminated/burrow-mottled grey clay

3.4 Palaeomagnetic methods and mineral magnetic parameters

PSV analysis: The discrete subsamples were analysed for natural remanent magnetisation (NRM) using a 2-G Enterprises model 755-R superconducting quantum interference device (SQUID) magnetometer with an automatic 3-axes stationary demagnetiser. The response of the samples to alternating field (AF) demagnetisation was measured using the same equipment, employing 5 milliTesla (mT) demagnetisation steps from 0 to 40 mT. These measurements were carried out within three months of core retrieval. PSV directional data were extracted using the "SQUID Tool v 2.0" program developed by Andreas Nilsson at Lund University. A least squares line and plane analysis (Kirschvink, 1980) was selected to determine characteristic remanent magnetisation (ChRM) from the demagnetisation steps, with 0% directional freedom and a specified desired mean angle of deviation (MAD) of less than 3.

Magnetic susceptibility (χ): Within one month of core retrieval, magnetic susceptibility of the discrete subsamples was measured using a Geofyzica Brno KLY-2 susceptibility bridge. The measured magnetic susceptibility was corrected for dry mass after freeze drying of the samples.

Anhysteretic remanent magnetisation (ARM): Samples were demagnetised along three orthogonal axes in consecutive order (X, Y and Z) in a 100 mT peak AF. ARM was then induced in a bias DC field of 0.1 mT superimposed on a peak AF of 100 mT that was cycled to 0 mT. ARM magnetisation was then measured using the SQUID magnetometer. Susceptibility of ARM (χ_{ARM}) was calculated by correcting for dry mass and the inducing field (Snowball, 1999).

Saturation isothermal remanent magnetisation (SIRM): A Redcliffe 700 BSM Pulse magnetiser was used to subject the discrete samples to a 1 T magnetic field. Room temperature SIRM was then measured using a Molspin Minispin fluxgate magnetometer. Mass specific SIRM (σ_{SIRM}) was later calculated after freeze drying of the samples.

Remanent Rotational Magnetism (RRM): The samples were first demagnetised along three orthogonal axes in consecutive order (X, Y and Z) in

a 100 mT peak AF. RRM was induced in a converted Molspin triple mu-metal shielded demagnetiser by rotating the samples on their Z-axis (the last to be demagnetised) at a frequency of 5 rps, perpendicular to the AF of 100 mT (Snowball, 1997). Magnetisation of the Z-axis was measured using the SQUID magnetometer. The three steps (demagnetisation, RRM induction, measuring magnetisation intensity) were then repeated, but by rotating the samples in the opposite direction when inducing RRM. RRM intensity for each sample was calculated as the difference between the magnetisation intensities measured for each rotation direction. This method removes the effect of any spurious ARM (Stephenson & Snowball, 2001). The *Bg* ratio, indicative of the effective biasing field, or gyro field, was calculated following Potter & Stephenson (1986):

$$Bg = b\,(ARM/RRM)$$

where b is the DC bias field used to induce ARM.

3.5 Lead (Pb) content and isotope analysis

Sediment from 52 selected discrete plastic cube subsamples from core 370530-5 was freeze-dried, milled and sent for Pb content and isotope analysis at the Department of Geography at Durham University, UK. Microwave acid extraction was used, with 5 ml H_2O, 8 ml HNO_3, 3 ml HCl and 2 ml HF. Analysis for isotopic composition was carried out on a Perkin Elmer Elan 6100 DRC Plus ICP Mass Spectrometer. Pb content was determined as the sum of all stable Pb isotopes.

3.6 Core correlation

LOI data were used for core correlation (Figure 2). Peaks and troughs in LOI data are in part due to annual and decadal changes in primary productivity throughout the Baltic Sea. Therefore, downcore LOI data show similar, synchronous patterns throughout the Baltic proper and offers an excellent independent method for core correlation within this area.

Sediment cores 370530-5 and 370540-6 were correlated to sediment core 372740-3 by way of the identification of 28 shared peaks and troughs in the LOI data, and linear interpolation was then applied between the identified points (Figure 2). Core 372740-3 was chosen as the master depth scale for plotting our results because, of the three cores, it has the highest resolution, covering the entire Littorina stage of the Baltic Sea, the relevant period of interest for our ΔR study. LOI data in the Baltic proper provides an excellent method for correlating sediment cores, which we utilise in this study to independently stack PSV data from multiple cores.

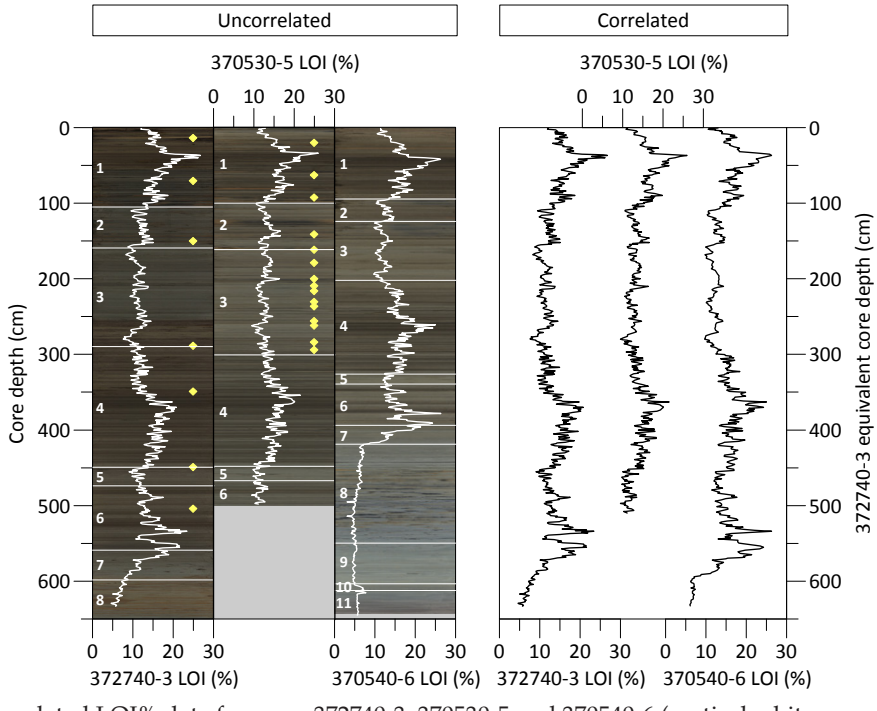

Fig. 2. Left: uncorrelated LOI% data for cores 372740-3, 370530-5 and 370540-6 (vertical white curves) superimposed on core photographs with numbered stratigraphical units and boundaries (white numbers and horizontal white lines). Intervals where foraminifera have been picked for ^{14}C analysis are also shown (yellow diamonds). Right: correlated LOI% data for cores 372740-3, 370530-5 and 370540-6 projected on a common 372740-3 depth scale.

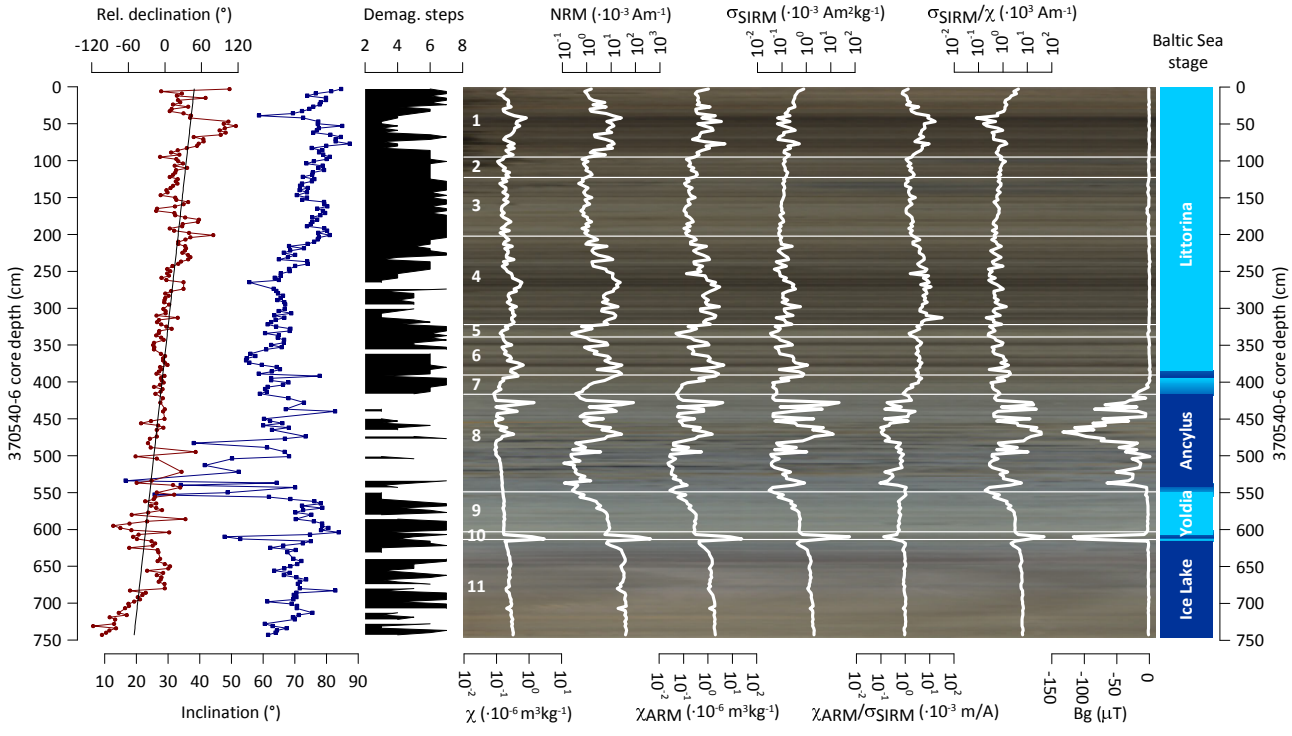

Fig. 3. Data from core 370540-6. Mineral magnetic data is superimposed on core photograph with numbered sedimentary units and boundaries (horizontal white lines and white numbers). For the colour version of this figure we refer to the online version. "Demag steps" denote number of demag steps used to calculate characersitic remanent magnetism (see methods).

3.7 Radiocarbon determinations

Benthic foraminifera were picked at IOW. The foraminifera samples were of the genus type *Elphidium*, mainly *Elphidium excavatum*, a euryhaline foraminifer suited to brackish conditions (Murray, 2006). Enough samples were picked to carry out ^{14}C dates at 23 depth intervals (Figure 2). Due to the lower salinity, foraminifera are much scarcer in the Baltic Sea than in the open ocean, so samples were generally picked where available in core 370530-5 and twin core 372740-3.

An effort was made to pick a higher concentration (ten samples) for the interval from 160 cm to 260 cm in core 370530-5, as this coincided with the estimated location of PSV declination feature *f* at 2.65 ka ago, according to one of our preliminary PSV age models. This also coincides with a feature in the ^{14}C calibration curve, known as the Hallstatt plateau (e.g. Van der Plicht, 2005). Our aim was to carry out wiggle match dating (WMD) of this feature to determine the ^{14}C reservoir age (e.g. Van Geel & Mook, 1989; Kilian et al., 1995), but due to the general scarcity of foraminifera we were ultimately not able to pick samples at a high enough resolution for the WMD exercise. However, due to the high sampling resolution we initially employed, sample sizes were considerably smaller for this interval.

^{14}C determinations on the foraminifer samples were carried out at the Lund University Accelerator Mass Spectrometry (AMS) laboratory when possible. Smaller samples, estimated to contain less than 100 μg C, were analysed at the Laboratory for Ion Beam Physics at Eidgenössische Technische Hochschule (ETH), Zürich. ETH employed an experimental, gaseous ^{14}C measurement technique whereby the samples are converted directly into CO_2, which is subsequently injected directly into a gas ion source for AMS measurements. The exclusion of the graphitisation step reduces the necessary sample size. This method is described in general by Ruff et al. (2010) and specifically in the case of foraminifera by Wacker et al. (submitted).

4. Results

4.1 Lithology

Sediment cores 370530-5, 370540-6 and 372740-4 are described using units 1-11, with unit divisions based on sediment type (Figures 2, 3 & 4 and Table 2). We only discuss the top 656 cm of core 372740-3, for which data are available.

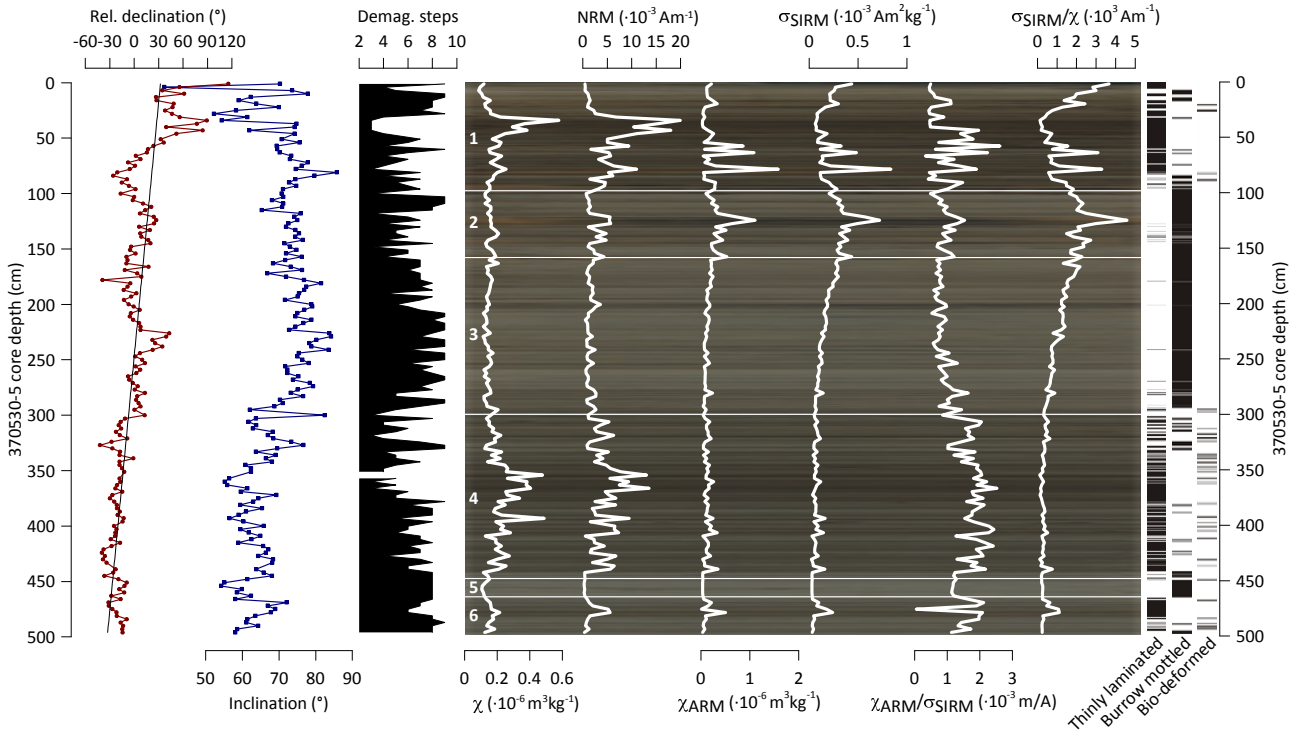

Fig. 3. Data from core 370530-5. Mineral magnetic data is superimposed on core photograph with numbered sedimentary units and boundaries (horizontal white lines and white numbers). For the colour version of this figure we refer to the online version. "Demag steps" denote number of demag steps used to calculate charactersitic remanent magnetism (see methods).

There is a distance of some 14 km between coring station 370530/372740 and coring station 370540, and we find the same Littorina units in all cores. However, units 2-7 account for 493 cm in the case of sediment core 372740-3 and only 321 cm for core 370540-6, suggesting that, in the case of those units, the sedimentation rate for coring station 370530/372740 is approximately 1.5 times greater than at station 370540. Similar sedimentation rate differences in the Gotland Deep have previously been reported by Christiansen et al. (2002). Such variations could influence the PSV lock-in delay for each core: this is the uncertain delay between sediment deposition and the geomagnetic field changes that are recorded as a detrital natural remanent magnetisation (NRM) as the sediments are progressively consolidated.

The units are interpreted as follows, from bottom upwards; Unit 11, a varved clay, is interpreted as being deposited during the Baltic Ice Lake stage. Unit 10, immediately above, is interpreted as representing the Baltic Ice Lake drainage stage. The Yoldia Sea stage is found in Unit 9 and is overlain by Unit 8, whereby the dark banded clay is interpreted as monosulphide banded clays deposited during the Ancylus Lake stage. Unit 7 is interpreted as the transitional phase from the Ancylus Lake stage to the Littorina Sea stage, a gradual transition owing to the slow breeching of the Drogden and Darß sills by eustatic sea level rise (Björck, 1995). Units 1-6 are interpreted as representing the Littorina stage of the Baltic Sea, with strongly laminated sediments present in units 1, 4 & 6. The laminations in Unit 1 are interpreted as coinciding with the Medieval Warm Period and those in units 4 & 6 with the Littorina maximum transgression (Zillén et al., 2008).

The fabric analysis done for core 370530-5 (Figure 3) agrees with the sedimentological interpretation described above. Thinly laminated sediment predominates in laminated units 1, 4 & 6, sporadically interrupted by minor episodes of burrow-mottled or bio-deformed sediment. Burrow-mottled sediment predominates in units 2, 3 & 5, with minor interruptions of thinly laminated sediment, especially in Unit 2. Almost no occurrences of bio-deformed sediment were noted in units 2, 3 & 5.

4.2 Loss-on-Ignition

LOI measured in units 8-11 is generally low and ranges between 3% and 8% (Figure 2). The highest value in these units, 7.8%, occurs in Unit 10, which was interpreted as representing the Baltic Ice Lake drainage event. A significant increase in LOI occurs

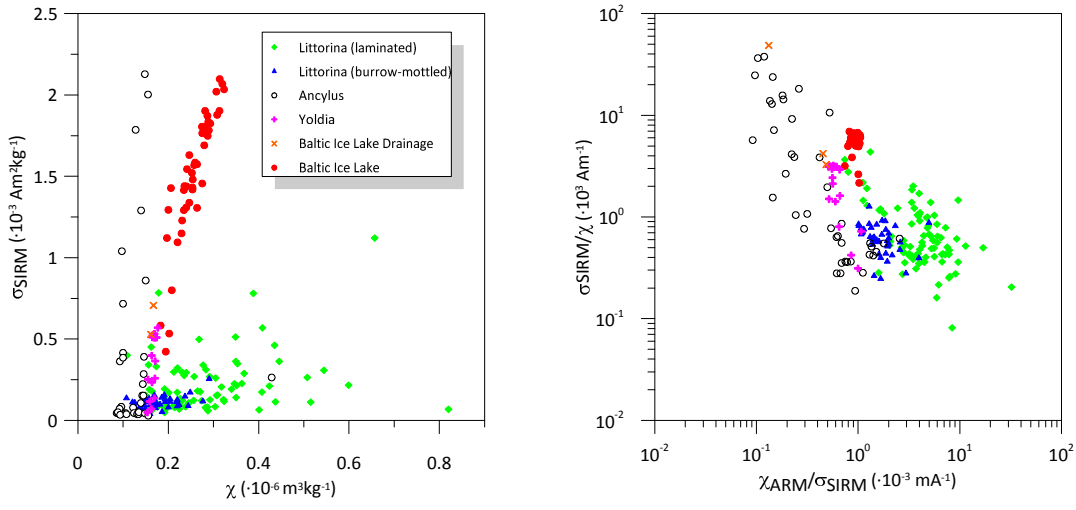

Fig. 5. Scatter plots of mineral magnetic data from core 370540-6 grouped by Baltic Sea stage of samples. Left: s SIRM vs c using a linear scale

in unit 7 during the transition from the Ancylus Lake to Littorina Sea stage. LOI in this transitional phase increases from a low of 8% to a high of 15%. LOI data in the Littorina Sea stage (Units 1-6) correlates to laminated sediment. Peak values in excess of 25% LOI are noted in the strongly laminated Units 1, 4 & 6, while generally lower LOI values of between 7.5% and 15% are noted in units 2, 3 & 5.

4.3 Mineral magnetic parameters

The mineral magnetic parameters described here for cores 370530-5 and 370540-6 are shown in Figures 3 & 4.

A very stable magnetic susceptibility signal of between 0.18 ·10^{-6} and 0.31 ·10^{-6} m^{3}kg^{-1} is found in Unit 11, gradually reducing in intensity up core. A peak of 2.91 ·10^{-6} m^{3}kg^{-1} is found in Unit 10, the Baltic Ice Lake drainage event. In the Yoldia Sea unit, Unit 9, magnetic susceptibility is low and declines from 0.17 ·10^{-6} to 0.15 ·10^{-6} m^{3}kg^{-1}. Ancylus Lake sediments (Unit 8) show a declining signal until the top half of the unit is reached, from 474 cm and upwards. Here, large peaks in magnetic susceptibility are found (maximum of 1.41 ·10^{-6} m^{3}kg^{-1}). The onset of the Littorina stage of the Baltic Sea (Unit 7) is represented by increasing values. Elevated values (>0.5 ·10^{-6} m^{3}kg^{-1}) are noted in Littorina Units 1, 4 & 6, where thinly laminated sediment is present. Littorina units 2, 3 & 5, containing mostly borrow-mottled sediment, display consistently lower values of between 0.1 ·10^{-6} and 0.5 ·10^{-6} m^{3}kg^{-1}. Units 1-6 in core 370540-6 contain generally higher values than core 370530-5, by a factor of approximately 1.3.

χ_{ARM} is particularly sensitive to stable single-domain (SSD) ferrimagnetic minerals. χ_{ARM} values in Unit 11 are generally stable and between approximately 1.0 ·10^{-3} and 2.0 ·10^{-3} m^{3}kg^{-1}. A large peak in χ_{ARM}, the highest recorded, of 24.2 ·10^{-3} m^{3}kg^{-1} is found in the Baltic Ice Lake drainage stage (Unit 10). Values generally decrease up core in Yoldia Sea stage Unit 9, reaching as low as 0.05 ·10^{-3} m^{3}kg^{-1}. In the Ancylus Lake stage Unit 8, peaks are once again encountered, with the highest being 4.01 ·10^{-3} m^{3}kg^{-1}. The transitional Unit 7 shows values as low as 0.06 ·10^{-3} m^{3}kg^{-1}, increasing steadily upwards towards the thinly laminated Unit 6, where peak values of up to 4.48 ·10^{-3} m^{3}kg^{-1} are present. The burrow-mottled Unit 5 displays lower χ_{ARM} values (order of magnitude 10^{-6}), leading into higher values, with a peak of 3.0 ·10^{-3} m^{3}kg^{-1}, in the thinly laminated Unit 4. Although, for this unit, elevated values are only found in core 370540-6 and not 370530-3. Generally lower χ_{ARM} values, between 0.103 ·10^{-3} and 1.10 ·10^{-3} m^{3}kg^{-1} are encountered in the burrow-mottled units 2 & 3. Peaks in χ_{ARM} values of up to 4.96 ·10^{-3} m^{3}kg^{-1} can be found in the lower part of Unit 1, coinciding with thinly laminated sediment.

σ_{SIRM} values, indicative of the ferrimagnetic mineral concentrations, generally mirror the trends seen in χ_{ARM}, with some differences in relative peak intensities, especially in the Ancylus Stage Unit 8. In Unit 11 we find generally stable σ_{SIRM} values between 2.1 ·10^{-3} and 0.58 ·10^{-3} Am^{2}kg^{-1}, decreasing steadily up core. A large peak of 59.5 ·10^{-3} Am^{2}kg^{-1} is found in Unit 10,

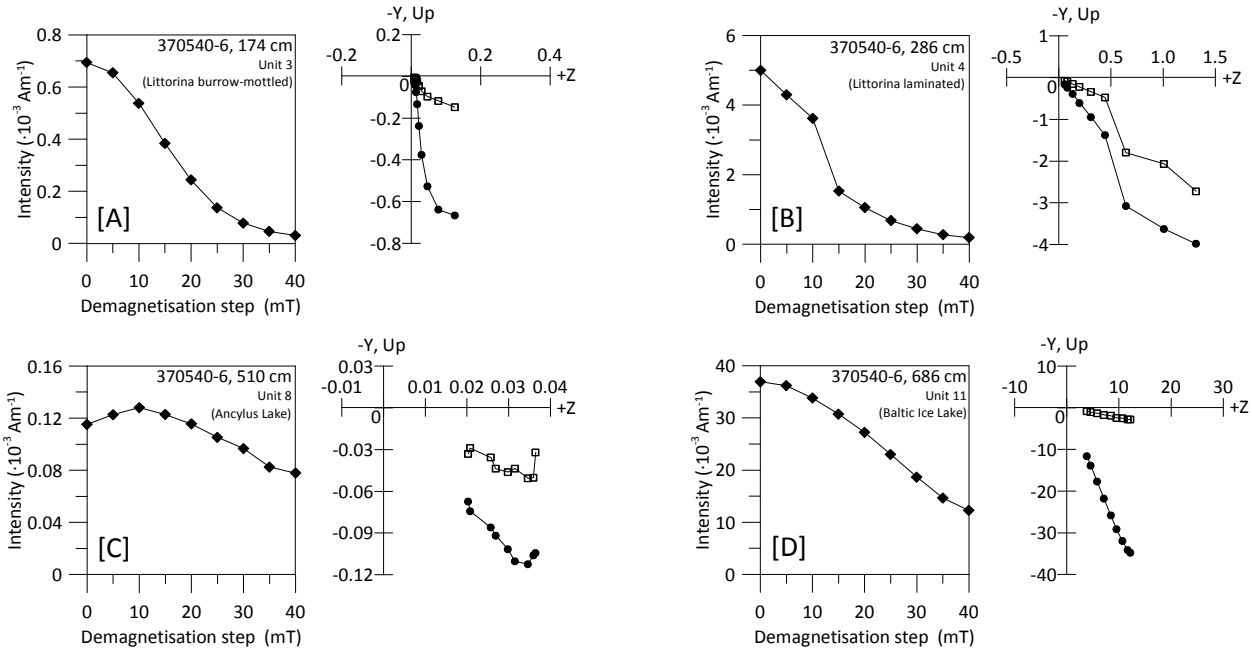

Fig. 6. Demagnetisation plots and associated Zijderveld plots for four selected samples from core 370540-6. [A]: sample from Littorina stage burrow-mottled sediment (unit 3). [B]: sample from Littorina stage thinly laminated sediment (unit 4). [C]: sample from Ancylus Lake stage sediment (unit 8). [D]: sample from Baltic Ice Lake stage sediment (unit 11).

the unit associated with the Baltic Ice Lake drainage event. σ_{SIRM} values in the Yoldia Sea Unit 9 are found to decrease upwards in the core, from $0.57 \cdot 10^{-3}$ to $0.048 \cdot 10^{-3}$ Am^2kg^{-1}. Elevated values are found in the Ancylus Stage Unit 8, peaking at $22.2 \cdot 10^{-3}$ Am^2kg^{-1}. The transitional Unit 7 shows generally lower values of between $0.34 \cdot 10^{-3}$ and $0.70 \cdot 10^{-3}$ Am^2kg^{-1}. Within the Littorina Units 1-6 generally higher values of up to $0.84 \cdot 10^{-3}$ Am^2kg^{-1} are noted in the laminated Units 1, 4 & 6, while the value of $0.30 \cdot 10^{-3}$ Am^2kg^{-1} is never exceeded in the burrow-mottled dominated sediments of Units 2, 3 & 5. Elevated values in Unit 4 are noted primarily in core 370540-6.

The χ_{ARM}/σ_{SIRM} ratio is indicative of magnetic grain size variations in situations where only one ferrimagnetic mineral dominates the mineral magnetic assemblage. In Unit 11 we find generally stable values around $1.00 \cdot 10^{-3}$ m/A. A negative excursion to $0.13 \cdot 10^{-3}$ m/A is found in Unit 10, the unit associated with the Baltic Ice Lake drainage event. The χ_{ARM}/σ_{SIRM} ratio in the subsequent Unit 9 are also found to be stable between $0.51 \cdot 10^{-3}$ and $0.67 \cdot 10^{-3}$ m/A, increasing in value to $1.08 \cdot 10^{-3}$ m/A just before the transition to Unit 8. In Unit 8, representing the Ancylus stage, we find various peaks and troughs, ranging between and $0.09 \cdot 10^{-3}$ and $2.57 \cdot 10^{-3}$ m/A. In Unit 7, the transitional phase between the Ancylus Lake and Littorina sea stages, we find a gradual up core increase from $0.99 \cdot 10^{-3}$ to $4.79 \cdot 10^{-3}$ m/A. Throughout the Littorina stage units 1-6, we find a generally higher χ_{ARM}/σ_{SIRM} ratio in the case of thinly laminated sediment units 1, 4 & 6, with peaks up to $32.5 \cdot 10^{-3}$ m/A. Generally lower values are found in the burrow-mottled sediment dominated units 2, 3 & 5, with values generally below $2.5 \cdot 10^{-3}$ m/A.

The σ_{SIRM}/χ ratio can be indicative of ferrimagnetic grain size when paramagnetic and diamagnetic materials do not make a significant contribution to measured χ, although potential complications arise when the magnetic assemblage contains more than one ferrimagnetic component. In Unit 11 there are stable values with an average value of $5.73 \cdot 10^3$ Am^{-1}. A large peak ($48.7 \cdot 10^3$ Am^{-1}) is found in the subsequent Unit 10, associated with the Baltic Ice Lake drainage event. Generally lower values, declining upwards from $3.1 \cdot 10^3$ to $0.31 \cdot 10^3$ Am^{-1} are found in the Yoldia Sea Unit 9. Large peaks of up to $37.7 \cdot 10^3$ Am^{-1} are encountered in Ancylus Lake Unit 8. We find lower values with an average of $0.67 \cdot 10^3$ Am^{-1} in Unit 7, the transitional phase to the Littorina Sea stage.

The effective gyro field, *Bg* ratio, shows large excursions to negative values lower than -100 μT in the Unit 8 Ancylus Lake stage sediments, with a maximum excursion to -132.7 μT noted at a depth of 468 cm.

Scatter plots of the magnetic data (Figure 5) were constructed to help in the identification of magnetic mineral properties. These show clear groupings

according to sediment units. σ_{SIRM} vs χ shows three clear linear trends; a steep trend which is dominated by Ancylus samples, a moderately steep trend dominated by Baltic Ice Lake and Yoldia samples, and a shallow trend dominated by Littorina samples. Some samples from the Baltic Ice Lake drainage stage and Ancylus stage with very high σ_{SIRM} values are not visible on the σ_{SIRM} vs χ scatter plot, due to the limited linear scale chosen. The scatter plot for σ_{SIRM}/χ vs χ_{ARM}/σ_{SIRM} shows three distinct groupings. In the top-left we see Ancylus and Baltic Ice Lake drainage stage samples, wit Baltic Ice Lake and Yoldia stage sediments in the centre. In the bottom right of the plot we see the Littorina sediment samples, with those from burrow-mottled sediments being closed to the centre than those from laminated sediments.

4.4 PSV analysis

4.4.1 Core 370530-5

The NRM intensity signal for this core (Figure 3) was found to vary between 0.23 $\cdot 10^{-3}$ and 19.94 $\cdot 10^{-3}$ Am^{-1}, depending on the sediment unit. The laminated Units 1, 4 & 6 were found to have higher, fluctuating NRM values, when compared to the lower, more constant values in burrow-mottled Units 2, 3 and 5. A peak value of 19.94 $\cdot 10^{-3}$ Am^{-1} was found in the uppermost Unit 1 and elevated values of up to 13.56 $\cdot 10^{-3}$ Am^{-1} were found in Unit 4. Units 2, 3 & 5 display an average value of 1.7 $\cdot 10^{-3}$ Am^{-1}.

Average inclination measured was 68.7°, which compares well to the expected geo-axial dipole (GAD) value of 72.3° for this latitude. The uppermost 50-75 cm of the core were observed to have high water content. The unconsolidated nature of this core interval made it difficult to preserve the directional integrity of the sediment during the subsampling process. The directional results for this interval are, therefore, more scattered and deemed to be unreliable. Downcore, we find two major groupings of high inclination (>80°) at 81 and 226 cm (Figure 3), as well as an isolated elevated value at 300 cm. Generally lower inclination values (<60°) can be found in the lower parts of the core between 300 and 500 cm. Where declination is concerned, we note a systematic linear trend in our data, which can be assigned to uncontrolled rotation of the gravity corer during retrieval. A 35° westerly swing in declination is noted at 226 cm, coinciding with the previously described inclination peak. This characteristic is interpreted as the declination swing from PSV feature *f* to feature *e* (Snowball et al., 2007). Furthermore, relative declination minima are noted at 81, 178, 327 and 436 cm, although we note that the minimum at 178 cm is based on a single point.

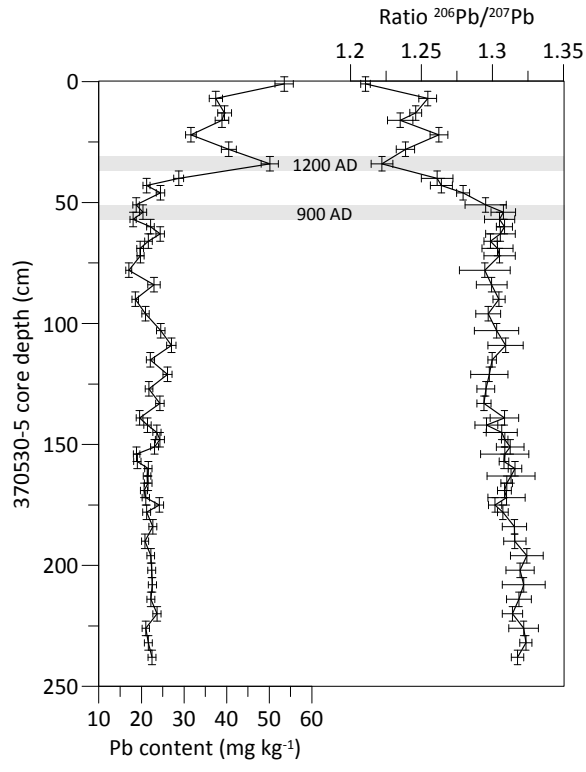

Fig. 7. Pb content (left) and $^{206}Pb/^{207}Pb$ isotope ratios (right) for samples from core 370530-5. Shaded intervals indicate indentified Medieval Pb pollution inception (900 AD) and peak (1200 AD).

The number of demagnetisation steps needed to calculate the ChRM is generally lower in thinly laminated sections of the sediment (Figure 3). When compared to the fabric analysis, the mean number of demagnetisation steps used to construct the directional signal was 5.8 in the case of thinly laminated and bio-deformed sediment, and 7.3 in the case of the burrow-mottled sediment dominated Units 2, 3 & 5. This observation suggests that more robust PSV data are ascertained from the burrow-mottled units in the Littorina sediments. For all Littorina sediments that we include in our palaeomagnetic stack, demagnetisation to 40 mT consistently removed in excess of 90% of the NRM.

4.4.2: Core 370540-6

Measured NRMs in this core (Figure 4) for the Unit 11 Baltic Ice Lake stage sediments show relatively steady values with an average value of 31.2 $\cdot 10^{-3}$ Am^{-1}. For Unit 10, interpreted as the Baltic Ice Lake drainage stage, we find a large peak of 410.9 $\cdot 10^{-3}$ Am^{-1}. Unit 9 Yoldia stage sediments display steadily decreasing NRM values up core, from 7.92 $\cdot 10^{-3}$ to 3.93 $\cdot 10^{-3}$ Am^{-1}. Unit 8 Ancylus stage sediments show very large peaks up to 83.9 $\cdot 10^{-3}$ Am^{-1} between 416 and 500 cm, with

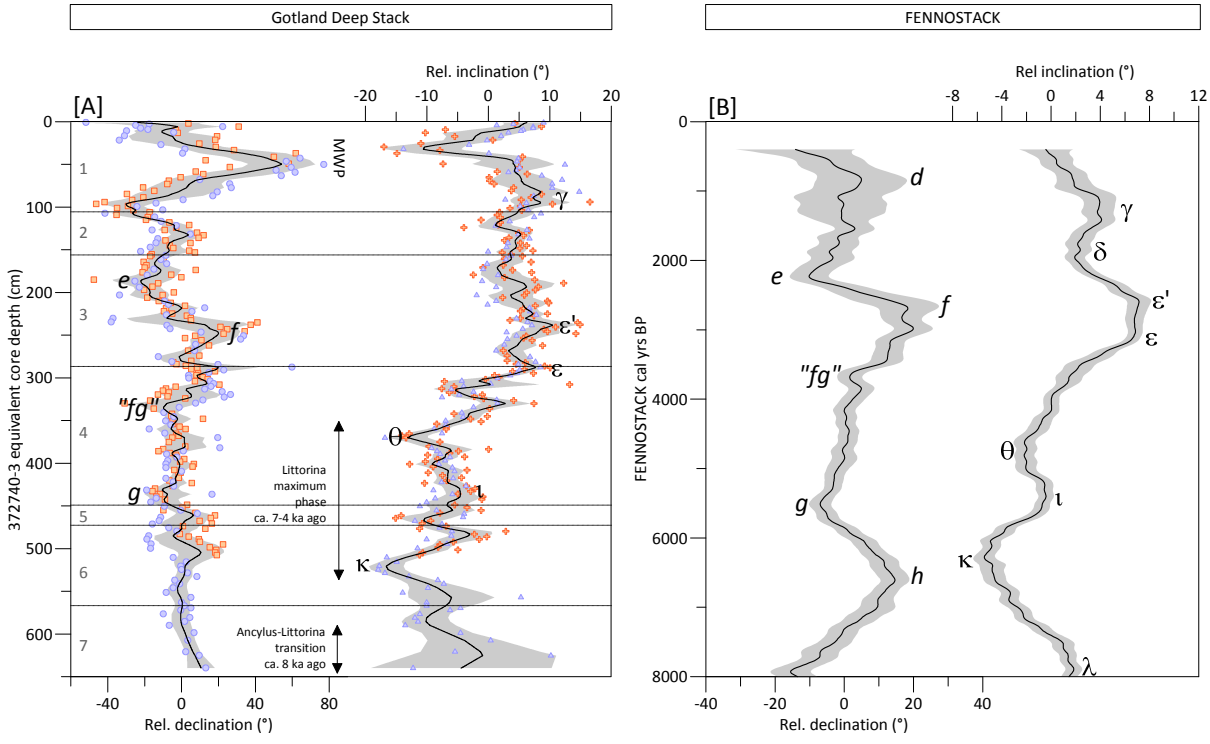

Fig. 8. [A]: Stacked relative declination and relative inclination data from cores 370530-5 and 370540-6 projected on shared 372740-3 depth scale. Shown is 370540-6 relative declination (blue circles), 370540-6 relative inclination (blue triangles), 370530-5 relative declination (orange squares) and 370530-5 relative inclination (orange crosses). Smoothed with 15-cm LOWESS smooth (black lines), with 95.4% confidence interval of smooth shown (grey band). Numbered sedimentary units shown for reference (grey numbers and horizontal grey lines). Approximate indications and ages of identified Baltic Sea lithological features added for temporal orientation. [B]: 150 year running window of FENNOSTACK master curve relative declination and relative inclination data. Grey bands represent 95.4% confidence intervals (data from Snowball et al., 2007).

generally lower values between 500 and 549 cm. Unit 7, the transitional unit between the Ancylus and Littorina stages, shows values climbing steadily up core, from 0.667 $\cdot 10^{-3}$ to 13.9 $\cdot 10^{-3}$ Am^{-1}. Measured NRM values for the Littorina stage sediments (Units 1-6) were found to be similar to core 370530-5. Laminated units 1, 4 & 6 show peaks of up to 26.2 $\cdot 10^{-3}$, 24.1 $\cdot 10^{-3}$ and 27.7 $\cdot 10^{-3}$ Am^{-1}, respectively, with burrow-mottled Units 2, 3 & 5 displaying lower values of 1.10 $\cdot 10^{-3}$ Am^{-1} on average.

Average inclination measured for this core was 69.3°, once again comparing well to the expected GAD value of 72.2° for this location. The uppermost 50-75 cm was found to be not well consolidated due to the high water content, which hampered accurate subsampling. Directional data for this interval are therefore deemed to be unreliable. Two major inclination peaks in the Littorina sediment can be identified at 77 and 195 cm depth (Figure 4). These peaks, while similar to those in core 370530-5, are somewhat less pronounced. As in core 370530-5, we note a systematic linear trend in our declination data (Figure 4), suggesting some form of core rotation during retrieval. A large swing in declination is noted from 201 to 147 cm depth, and we interpret this as the westerly declination swing from PSV feature *f* to *e*, however, it is less clear than was the case in core 370530-5.

Generally, more robust PSV data, as shown by the higher number of demagnetisation steps used to construct directional data, is found in burrow mottled Littorina Units 2, 3 & 5 than in Littorina Units 1, 4 & 6, which are dominated by thinly laminated sediment. Zijderveld and demagnetisation plots for typical Littorina Stage samples are shown in Figures 6A and 6B. In Figure 6A a more robust sample from the burrow-mottled Littorina Unit 3 is shown, where a single ChRM can clearly be identified. The Kirschvink (1980) analysis procedure with a specified MAD of <3 resulted in the demagnetisation steps from 5 mT to 40 mT being used to determine the ChRM and directional data for this sample. In Figure 6B a sample from the thinly laminated Littorina Unit 4 is shown. The NRM for this sample can be broken down into two components. One component is relatively soft and is removed by demagnetization fields up to and including 15 mT, leaving a harder component that is practically demagnetised at 40 mT. The Kirschvink

(1980) analysis procedure with a specified MAD of <3 resulted in the demagnetisation steps from 15 mT to 40 mT being used to determine the ChRM and directional data for this sample. These examples show the importance of demagnetising samples and employing an objective analytic procedure to correctly identify a ChRM. All Littorina samples (the period covered by our palaeomagnetic age model) displayed in excess of 90% removal of NRM intensity at 40 mT demagnetisation.

The short transitional Unit 7 between the Ancylus and Littorina stages also yields robust PSV data. Poor PSV data, indicated by large variations in directional data and poor identification of a ChRM, are found in the Ancylus Unit 8 (Figures 4 & 6C).

Units 9, 10 and 11 which represent the Yoldia Sea, Baltic Ice Lake drainage and Baltic Ice Lake stages, respectively, contain a mixture of robust PSV data whereby five or more demagnetisation steps could be used to construct the directional data (Figure 6D), as well as some less robust data whereby less than five steps were used. On average, 4.7 demagnetisation steps were required to construct the ChRM for these units. A relatively steady inclination signal can be noted for these units, with the exception of Unit 10, which is associated with the Baltic Ice Lake drainage stage.

4.5 Lead content analysis

Results for both Pb content and $^{206}Pb/^{207}Pb$ in core 370530-5 (Figure 7) show a marked shift between 54 and 34 cm. Here we see an increase in Pb content from approximately 20 to 50 mg·kg^{-1}, accompanied by a drop in the $^{206}Pb/^{207}Pb$ ratio from approximately 1.31 to 1.22. Pb content falls back to 30 mg·kg^{-1} at 22 cm depth, accompanied by a $^{206}Pb/^{207}Pb$ ratio increase to 1.26. Pb content increases again near the top of the core, with an associated shift in the $^{206}Pb/^{207}Pb$ ratio. However, as the gravity coring process leads to the loss of the uppermost 30 cm or so of sediment, we are not able to assess how this pattern continues.

4.6 Radiocarbon determinations

Of the 23 foraminifera samples submitted for ^{14}C analysis, 22 resulted in successful ^{14}C determinations (Table 3). Of these, 13 samples were of sufficient mass to be analysed using the standard AMS technique (LuS analyses), all of which resulted in a successful analysis. Two of the AMS determinations resulted in an error of ≥100 years (1σ), both of which were less than 1000 µg in mass, and therefore nearing the limits of the AMS technique with a standard graphitisation process.

The other 10 samples of foraminifera were those that were initially picked for WMD and had much lower masses, containing between 4 and 100 µg carbon. These were analysed using the experimental gas ion source technique (ETH analyses). One of these determinations failed to produce a result and, of the remaining nine, six resulted in a 1σ error of ≥100 years. These six samples all had a mass of <200 µg (24 µg carbon), leading to relatively large errors due to poor counting statistics (caused by the low amount of ^{14}C) and increased sensitivity to contamination during preparation. It is noted that, for samples in the 500-1000 µg range, the experimental gas ion source technique (ETH analyses) yields generally smaller errors than the standard AMS method with graphitisation (LuS analyses). However, this could be due to differing conventions for reporting errors between laboratories. We have used all but two determinations for inferring ΔR. Determinations ETH-41827.1.1 and ETH-41829.1, which were carried out on exceptionally small samples, yielded weak currents during ^{14}C analysis - a factor of two lower than the standard and blank measurements used. We do not include these two ^{14}C determinations in our ΔR study.

5. Independent PSV & Pb age model and ΔR inference

5.1 Gotland Deep stacked PSV record

In order to enable a more robust identification of PSV features, a Gotland Deep stacked PSV record for cores 370530-5 and 370540-6 was created (Figure 8A). This stacked PSV record covers only the most recent Littorina Stage (8 kyr ago to present day) of the Baltic Sea, i.e. the uppermost Units 1-6 in our study (Figures 2, 3 & 4, Table 2). These Littorina Stage sediments cover the whole period of interest for our ΔR study, seeing as all our ^{14}C determinations on foraminifera are from Littorina Stage sediments. As previously discussed, these sediments produced the most consistently robust PSV data, whereby demagnetisation to 40 mT consistently removed 80%-90% of the NRM. The PSV data from the two cores is stacked using LOI correlation as an independent stacking method. In palaeomagnetic studies where no independent stacking method is available, such as when comparing individual lake records, PSV data is often stacked by way of drawing tie lines between various records displayed side-by-side, which can introduce an interpretation bias. We take advantage of independent core correlation using LOI in the Baltic Sea to produce a robust stack.

The stack was produced as follows: The linear

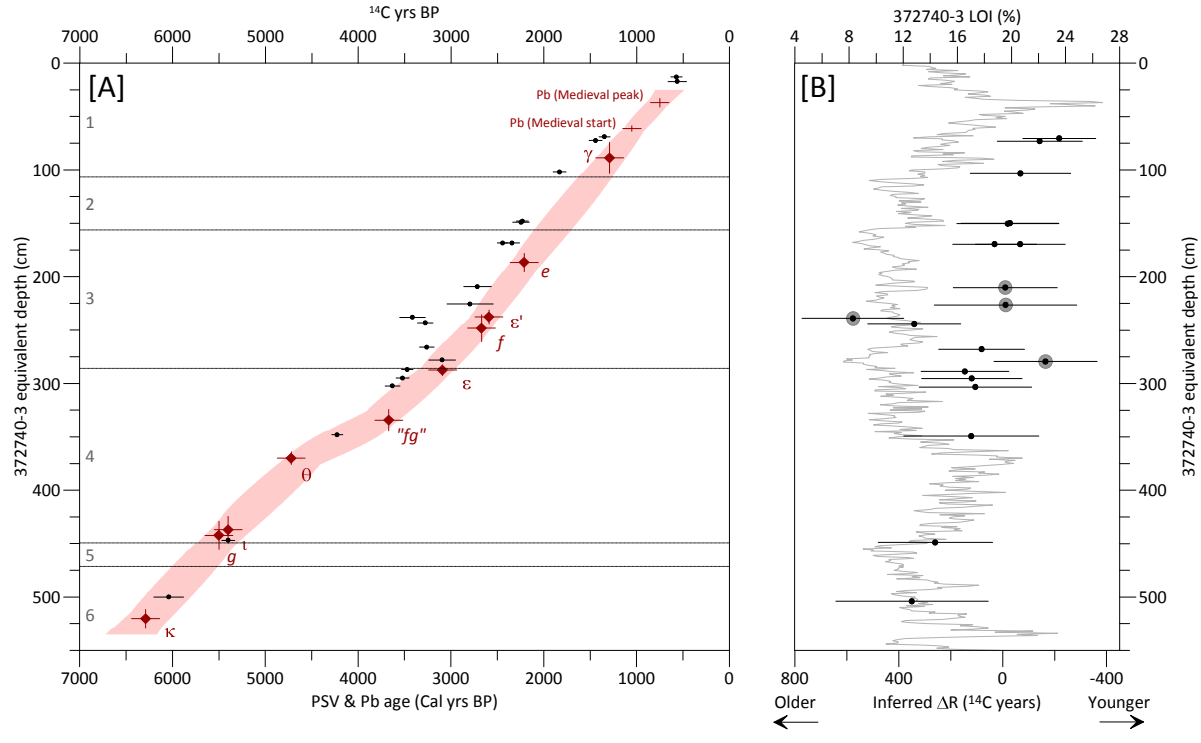

Fig. 9. [A]: 68.2% confidence interval for PSV & Pb depositional age model (light red shaded area) and associated PSV (red diamonds) & Pb (red crosses) age constraints with 1 sigma errors. 14C determinations on foraminifera with 1 s errors (black circles). Numbered sedimentary units shown for reference (grey numbers and horizontal grey lines). [B]: inferred Delta-R values for ^{14}C determinations with 1 sigma error (black triangles). Filled grey circles denote Delta-R values based on ^{14}C determinations with a total sample mass of less than 200 mg. LOI% data (light grey curve) for core 372740-3 shown for reference. All data projected on 372740-3 depth scale. For the colour version of this figure we refer to the online version.

trends noted in the declination data for the two cores (Figures 3 & 4) were removed. PSV directional data from cores 370530-5 and 370540-6 were subsequently rotated to zero and projected onto the shared 372740-3 depth scale using the LOI correlation discussed earlier (Section 3.6 & Figure 2). The stacked dataset is terminated at 650 cm core depth, as this level is below the Ancylus-Littorina transition, meaning that our stacked data only covers the Littorina stage sediments. The stacked record was smoothed using a locally weighted scatterplot smooth (LOWESS) with a 15 cm smoothing window. 1σ confidence intervals for the smoothed dataset were calculated using statistical bootstrapping. The stacked dataset is shown in Figure 8A, where sediment unit boundaries have been added for reference. We have also indicated the approximate intervals for the Littorina/Ancylus transition, Littorina maximum and Medieval Warm Period (MWP) in the stack, to give some form of general time constraint before attempting to identify PSV features.

PSV features in the resulting smoothed dataset were then compared to those present in the FENNOSTACK master curve (Snowball et al., 2007) shown in Figure 8B. Six inclination and three declination features from FENNOSTACK were identified (Figure 8A and Table 4). Additionally, an unlabelled declination swing in FENNOSTACK that we have also identified in the Gotland Deep stacked PSV record is included as a fourth identified declination feature. It is referred to here as "fg". Ages and associated age errors for the resulting PSV age constraints were transferred from the FENNOSTACK chronology. Depth errors for the age constraints are based on the sampling resolution (±1.5 cm), estimated core correlation error (±1 cm) and an interpretation error for each identified PSV age constraint. This interpretation error was determined using the 1σ confidence intervals of the smoothed Gotland Deep stacked PSV record.

5.2 Lead chronology age constraints

The increase in Pb content and concomitant shift in $^{206}Pb/^{207}Pb$ ratio, which we identified from 54 to 34 cm in core 370530-5 (see Section 4.5), are attributed to Pb pollution during the Medieval period (Brännvall et al., 2001; Renberg et al., 2001; Zillén et al., 2012). We use this historically dated feature to construct two

age constraints, with ages following the Pb analysis of varved lakes in northern Sweden by Brännvall et al. (2001); we select a date of 900AD (1050 cal yr BP) for the beginning of the decrease in the $^{206}Pb/^{207}Pb$ ratio at 54 cm in core 370530-5, and 1200AD (750 cal yr BP) for the peak in Pb content (and associated trough in the $^{206}Pb/^{207}Pb$ ratio) at 34 cm in core 370530-5 (Figure 7). The depths are transferred to the 372740-3 depth scale following the LOI correlation (Table 4). There is still some uncertainty regarding the exact timing of the peak so we have therefore assigned a conservative uncertainty of ±100 years. The assigned depth errors for the two points are based on the sampling resolution and an additional 1 cm error attributed to the transfer from the 370530-5 to the 372740-3 depth scale.

We have not been able to identify the modern Pb peak associated with the use of lead enriched petrol up until the 1970s, nor the Pb pollution peak associated with the Roman period. In the case of the modern peak, the top most sediments have simply been lost due to the gravity coring process. We expect that this peak should be found if an overlapping short-core were to be used, as in the case of Zillén et al. (2012). We were unable to conclusively identify the Roman pollution peak, probably due to the large distance from the point source of the pollution. However, in those parts of the core where we might expect to find the Roman pollution peak (approx 100-200 cm depth, see Figure 7), we find Pb concentration and $^{206}Pb/^{207}Pb$ ratios in a similar range as those encountered by Zillén et al. (2012) for the Roman period.

We note large changes in LOI in our cores, changes which we have used for correlation. Such a change in organic matter could theoretically affect the recording of the Pb pollution signal in the sediment cores. It is for this reason that we have also analysed the $^{206}Pb/^{207}Pb$ ratio, which should be unaffected by changes in organic matter. Renberg et al. (2001) reports that changes in organic matter, such as a transition to peat layers, does not affect the identification of the Pb pollution history. Zillén et al. (2012) successfully developed Pb isochrones for the Baltic Sea and carried out a detailed examination of the Pb concentration and Pb isotope ratio data across boundaries between Baltic Sea sediment of high and low organic matter, such as the transition from laminated sediments to burrow-mottled sediment. They found that such transitions produced no significant changes in Pb data, thus increasing confidence in the identification of the Pb pollution signal in Baltic Sea sediments.

5.3 Combined PSV & Pb age model

Calendar age constraints and associated errors (Table 4) produced by the Gotland Deep stacked PSV record and the atmospheric Pb analysis are included in a Bayesian depositional age model using OxCal version 4.1 (Bronk Ramsey, 2008; Bronk Ramsey, 2009). While OxCal is primarily a tool for ^{14}C calibration, we use it here only to construct our independent PSV & Pb age model and we do not include any ^{14}C information whatsoever. The resulting age model with 1σ age range is shown as the shaded area in Figure 9A. More detailed information regarding the construction of this OxCal depositional age model is provided as supplementary information.

5.4 Inferred ΔR

ΔR represents the ^{14}C year offset from the global Marine09 (Reimer et al., 2009) calibration curve, whereby the global marine reservoir is calculated using an ocean-atmosphere box diffusion model (Stuiver and Braziunas, 1993; Hughen et al., 2004). ΔR=0 is equivalent to an absolute reservoir age of approximately 400 years (e.g., ΔR=-100 is equivalent to approximately 300 years).

We compare our ^{14}C determinations on foraminifera to the PSV & Pb age model to infer ΔR. Each ^{14}C determination on foraminifera ($^{14}C_{FORAM}$) is assigned a calendar age (t) with 1σ error, based on the PSV & Pb age model. This independent calendar age is then assigned a corresponding normal distribution which is then folded by the Marine09 calibration curve to produce an expected Marine09 ^{14}C age distribution ($^{14}C_{M09}$) associated with the assigned calendar age (t) for each ^{14}C determination ($^{14}C_{FORAM}$). This method can be approximately described as a "reverse calibration" of the known calendar age into expected ^{14}C years. While this is more complex than simply looking up corresponding ages on the calibration curve, it gives a more realistic result. We infer ΔR by calculating the relative offset from the Marine09 calibration curve as follows:

$$\Delta R = {}^{14}C_{FORAM}(t) - {}^{14}C_{M09}(t)$$

1σ errors for ΔR have been calculated by a propagation of the 1σ errors associated with $^{14}C_{FORAM}(t)$ and $^{14}C_{M09}(t)$. Our ΔR values vs 372740-3 core depth are shown in Table 3 and Figure 9, with LOI data shown in the figure for comparison with other Baltic Sea records. For comparison with records from outside the Baltic Sea, ΔR values are also plotted against calendar age in Figure 10, whereby core depth has been converted to calendar age using the PSV & Pb age model, with associated 1σ errors.

Uncertainties surrounding the PSV method, specifically the lock-in delay of the NRM, make it

B.C. Lougheed et al. (2012), doi:10.1016/j.quascirev.2012.03.013

Table 3. ^{14}C determinations on foraminifera samples from cores 370530-5 and 372740-3 with associated PSV & Pb ages and inferred ΔR.

Core	370530-5 depth (cm)	372740-3 (equiv.) depth (cm)	Foraminifera genus	Total sample mass (µg)	Sample code	^{14}C age (^{14}C yrs BP ±1σ)	PSV & Pb age (Cal yrs BP ±1σ)	Expected Marine09 ^{14}C age (^{14}C yrs BP ±1σ)	Inferred ΔR (^{14}C yrs BP ±1σ)
372740-3	-	13 - 15	Elphidium	2400	LuS-9514	570 ±60	Out of range	-	-
370530-5	19 - 21	(17.2 - 20)	Elphidium	700	LuS-9126	560 ±100	Out of range	-	-
370530-5	62.6 - 63.5	(72.5 - 73.7)	Elphidium	1500	LuS-9127	1440 ±70	1112 ±142	1563 ±127	-218 ±140
372740-3	-	69 - 72	Elphidium	1900	LuS-9515	1345 ±60	1135 ±145	1583 ±148	-143 ±164
370530-5	91 - 94.2	(102 - 104.6)	Elphidium	1800	LuS-9128	1830 ±70	1416 ±180	1899 ±180	-69 ±193
370530-5	140 - 142.7	(149 - 151.7)	Elphidium	600	LuS-9129	2245 ±90	1846 ±203	2258 ±176	-28 ±188
372740-3	-	148 - 152	Elphidium	1300	LuS-9516	2230 ±65	1850 ±203	2265 ±175	-20 ±197
370530-5	160.5 - 162.8	(168.5 - 170.6)	Elphidium	519	ETH-41826.1.1	2343 ±83	2026 ±195	2411 ±151	-68 ±172
370530-5	160.5 - 162.8	(168.5 - 170.6)	Elphidium	468	ETH-41826.1.2	2442 ±87	2026 ±195	2411 ±151	31 ±161
370530-5	178 - 180	(185 - 187.8)	Elphidium	50	ETH-41827.1.1[a]	3558 ±193	-	-	-
370530-5	199.3 - 201	(209.3 - 211.1)	Elphidium	92	ETH-41828.1.1	2714 ±148	2396 ±180	2724 ±135	-10 ±200
370530-5	208.5 - 210.5	(219.2 - 221.4)	Elphidium	36	ETH-41829.1.1[a]	2764 ±393	-	-	-
370530-5	215 - 217	(225.6 - 227.3)	Elphidium	48	ETH-41830.1.1	2794 ±249	2537 ±173	2805 ±114	-11 ±274
370530-5	229.5 - 231.5	(238.2 - 239.9)	Elphidium	144	ETH-41832.1.1	3413 ±138	2643 ±163	2837 ±139	576 ±196
370530-5	235.5 - 237.5	(243.4 - 245.1)	Elphidium	538	ETH-41833.1.1	3276 ±82	2703 ±172	2936 ±159	340 ±179
370530-5	255 - 257	(266 - 270)	Elphidium	937	ETH-41834.1.1	3260 ±79	2952 ±201	3179 ±145	81 ±165
370530-5	261 - 263	(278 - 280.7)	Elphidium	120	ETH-41835.1.1	3094 ±143	3072 ±197	3259 ±138	-165 ±199
370530-5	283.5 - 284.5	(295 - 295.8)	Elphidium	1300	LuS-9130	3520 ±70	3182 ±197	3325 ±158	145 ±169
372740-3	-	287 -290.5	Elphidium	2500	LuS-9517	3470 ±60	3279 ±218	3401 ±180	119 ±193
370530-5	293 - 295.5	(302.4 - 304.3)	Elphidium	800	LuS-9131	3630 ±80	3382 ±230	3525 ±201	105 ±216
372740-3	-	348 - 350.5	Elphidium	2500	LuS-9518	4225 ±60	4118 ±337	4104 ±253	121 ±260
372740-3	-	447 - 451	Elphidium	1800	LuS-9519	5400 ±70	5510 ±220	5141 ±209	259 ±220
372740-3	-	500 - 508	Elphidium	800	LuS-9520	6040 ±160	6100 ±253	5691 ±246	349 ±293

[a] denotes ^{14}C determinations that have been rejected (Section 4.6 in text).

difficult to infer absolute Gotland Deep ΔR values downcore, with errors greater than 300 years for some of our ΔR estimates. However, Littorina temporal changes in ΔR are found to occur within a range of approximately 800 years, although this is exaggerated somewhat by a single ΔR value of 576 ±196 associated with determination ETH-41832.1.1, which was one of the lower mass samples with a mass of less than 200 µg. If we disregard its inferred ΔR value, the range of ΔR changes is in the order of approximately 570 years, although when one considers the errors associated with the individual ΔR values this range becomes larger. A general upcore trend towards younger ΔR values upwards in the core is seen. We note that it was not possible to calculate ΔR values for the two uppermost ^{14}C determinations (LuS-9514 and LuS-9126), as these fall outside the range of our PSV & Pb age model.

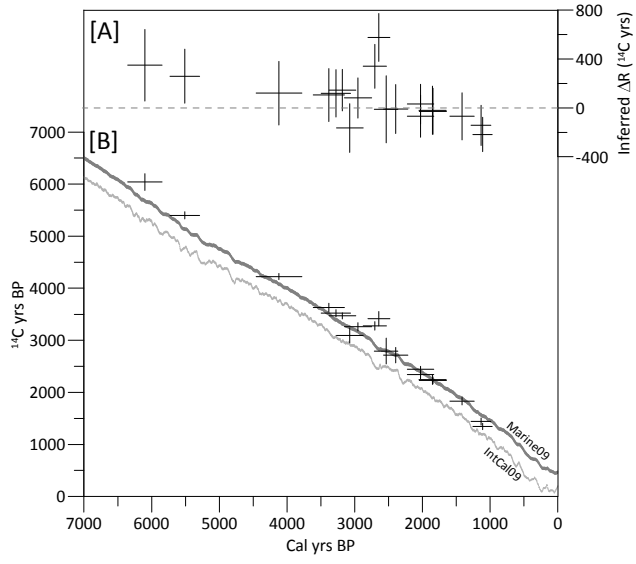

Fig. 10. [A]: inferred DR values of foraminifer samples. Depth values have been converted to cal yr BP using PSV & Pb age model. [B]: measured 14C ages of foraminifer samples. Depth values have been converted into cal yr BP using PSV & Pb age model. IntCal09 and Marine09 curves (Reimer et al., 2009) shown for reference. All errors shown in this figure are 1 ssigma .

6. Discussion

6.1 Mineral magnetic parameters

Based on our mineral magnetic measurements, we propose differing minerals as the dominant carriers of the NRM signal in the various sediment units. We hypothesise the following assemblages for the different sediment types in the σ_{SIRM} vs χ scatter plot (Figure 5): The Ancylus Lake samples, displaying a steep linear trend on the scatter plot, are interpreted as ferrimagnetic iron sulphide bearing, most likely greigite (Fe_3S_4) (Snowball and Torii, 1999). Additionally, the Baltic Ice Lake drainage samples have high σ_{SIRM}/χ ratios consistent with greigite. Yoldia Sea and Baltic Ice Lake samples, which display a moderately steep linear trend on the σ_{SIRM}/χ scatter plot, are interpreted as bearing multi-domain (MD) magnetite, most likely detrital in origin. Littorina stage samples occupy the shallow linear trend on the σ_{SIRM} vs χ scatter and we suggest this as possibly being due to the presence of stable single-domain (SSD) magnetic grains, but more research is necessary to establish their mineralogy and origin, as multiple magnetic minerals may be present here. The σ_{SIRM}/χ vs χ_{ARM}/σ_{SIRM} scatter plot (Figure 5) shows a clear trend from top-left to bottom-right. We attribute this to the dominance of ferrimagnetic iron sulphide (e.g. greigite) grains in the top-left region of the plot, MD magnetite grains in the centre region, and finer SSD grains in the bottom right area of the plot. In both scatter plots we find that the samples associated with laminated Littorina sediment occupy a wide range of values, so it is possible that laminated sediments can contain different mineral magnetic assemblages on a lamination scale.

Our interpretation that Ancylus Lake stage and Baltic Ice Lake drainage stage samples are ferrimagnetic iron sulphide bearing, and most likely greigite bearing, is supported by our measurement of the effective gyro field (*Bg* ratio, Figure 4). The negative excursions in both these core intervals are consistent in value with those ascertained by Snowball (1997) for greigite bearing samples at low rotation rates. Additionally, they often occur where monosulphide banding, consistent with greigite, is noted in the sediment. It should be noted that these negative values in *Bg* ratio generally correlate with negative excursions in χ_{ARM}/σ_{SIRM} ratio, as well as peaks in χ_{ARM} and σ_{SIRM}, which, when occurring concomitantly, are also indicative of greigite. While these measurements most likely indicate the presence of greigite, more detailed investigations regarding the presence of greigite in Ancylus Lake sediments can be found in previous studies, where it is concluded that greigite precipitated post-depositionally in the Ancylus Lake clays due to the diffusion of sulphide from the overlying Littorina stage sediments (e.g. Sohlenius, 1996; Kortekaas, 2007).

6.2 Palaeomagnetic secular variation (PSV)

Despite a factor 1.5 difference in sedimentation rate between the two cores, the stacked inclination and declination datasets for the two cores both show similar trends in both inclination and declination data. However, an offset in declination data can be noticed between the two cores in the intervals 0 - 100 cm and 450-500 cm in the stacked dataset (Figure 8A). As this occurs near the top and bottom of the core record in 370530-5, we attribute it to increased core rotation at

the end of the gravity core barrel. We do not find the same offset in the inclination data, which are similar for both cores. We conclude that, despite the difference in sedimentation rate between the two locations, there does not appear to be a relative difference in PSV lock in delay for the two cores.

Due to the moderate quality of the PSV data ascertained from our Baltic Sea cores, our PSV age constraints result in quite large errors, both in terms of absolute age and depth interval in the core. Kotilainen et al. (2000), who also produced a PSV age model for Gotland Deep sediments, proposed significantly smaller errors. We are less optimistic that such accuracy can be achieved. Nevertheless, due to a lack of other useful, independent methods that can be used to date Baltic Sea sediments and compared to ^{14}C chronologies, our PSV age constraints provide a functional dating method, especially when PSV records from multiple cores are stacked.

We find moderate to good PSV data in the Littorina stage sediments included in our stacked dataset, with generally poorer directional data occurring in thinly laminated sediment than in burrow-mottled sediment, as indicated by the lesser number of magnetisation points used to construct the PSV data for thinly laminated intervals (Figure 3). Generally, the more intensely laminated the sediment, the poorer the PSV data, reaffirming that more research is needed into the mineral magnetic properties of the laminated sediment units. In Ancylus stage sediments, which fall outside of our stacked PSV dataset, we find very poor data, which is brought about by the iron sulphide bearing sediments characteristic of this interval. Stephenson and Snowball (2001) previously showed that greigite (an iron sulphide) bearing sediments acquire a large gyromagnetic magnetisation (GRM) during static AF demagnetisation. Due to the possibility that greigite is responsible for this GRM, we can suspect that the NRM for these sediments is a secondary chemical remanent magnetisation (CRM) of theoretically unknown age, which makes Ancylus stage sediment unreliable for palaeomagnetic dating purposes. Figure 6 shows Zijderveld and demagnetisation plots from an Ancylus stage sample in core 370540-6 at 510 cm, where a similar gyromagnetic effect can be seen as an acquisition of magnetisation intensity during static AF demagnetisation. A true GRM signal cannot be seen in the Zijderveld plot for the demagnetisation steps analysed, as it is likely obscured due to the presence of other magnetic minerals in the sample. However, the sample is clearly unsuitable for reconstructing trends in PSV.

A previous study of Baltic Sea sediments by Kochegura (1992) noted a substantial decrease in inclination values by over 50° at 2.8 ka ago. This decrease, despite being based on only three measurement points, was interpreted by Dergachev et al. (2008) as evidence of the "Sterno-Etrussia" geomagnetic excursion (Nöel & Tarling, 1975). We note that our high-resolution stacked dataset shows no such negative decrease in inclination values at that interval (between approx 250 and 300 cm in Figure 8A), nor is this proposed excursion found in FENNOSTACK (Figure 8B) (Snowball et al., 2007).

Below the cut-off point for our stacked data, in the bottom (Unit 11) of core 370540-6 (Figure 4), a notable large eastward declination swing of approximately 120° is found between 674 cm and 743 cm, although this is reduced to approximately to 90° when the linear trend noted in our declination data is removed. A similar eastward declination swing of approximately 90° was also noted by Björck and Sandgren (1986), Björck et al. (1987) and Ising (2001) when reconstructing PSV for ^{14}C and varve dated lakes in southern and central Sweden. In those studies, the declination swing was dated to between 11,500 and 10,200 ^{14}C years BP. Assuming this is the same declination swing as the one present in Unit 11, the aforementioned dates agree with our interpretation of Unit 11 as being Baltic Ice Lake stage sediment. Combined with the steady NRM signal and robust directional data (Figure 6) found in this unit, we propose that Baltic Ice Lake sediment can be a useful source for Late Weichselian PSV reconstructions.

6.3 Geochronology

For the purpose of calculating an inferred ΔR for individual ^{14}C determinations, we assume that the PSV & Pb age model is representative of calendar ages. However, it is possible that the PSV age constraints are influenced by a change in lock-in delay associated with a change in sedimentation rate between the laminated and burrow-mottled units. However, as was noted in the results section, there is minimal offset between the stacked PSV data for the cores 370530-5 and 370540-6, despite the 1.5 factor difference in sedimentation rate for the two sites. Nevertheless, downcore PSV lock-in delay changes, such as those due to change in sediment type, could contribute to a perceived amplification in sediment rate change. In addition, as discussed in Section 6.1, the magnetic assemblage can differ between sediment types and could potentially contribute to a change in lock-in delay. The existence of a PSV lock-in delay and/or variation thereof cannot be ruled out and we have not been able to prove otherwise. Consequently, we have assigned conservative age and depth errors for the PSV age constraints used in the PSV & Pb age model.

We note that the PSV & Pb age model indicates realistic changes in sedimentation rate (Figure 9) between laminated and burrow-mottled sediment, with a generally higher sedimentation rate during laminated intervals. Of particular note is the reduced sedimentation rate between 375 cm and 325 cm depth, which coincides with a sudden drop in LOI values. It is possible that a similar change in sedimentation rate occurs at the drop in LOI values between 35 and 15 cm, but our PSV & Pb age model does not extend this far.

Below the reach of our geochronologies shown in Figure 9, the Ancylus-Littorina (A-L) transition occurs at approximately 575 cm on the 372740-3 depth scale. The PSV & Pb age model does not extend down this far, but it suggests at least that the 6.5 ka age for the A-L transition produced by OSL dating carried out by Kortekaas et al. (2007) in the Arkona Basin may be too young. This agrees with the findings of Rößler et al. (2011), who found older ages than Kortekaas et al. (2007) for the A-L transition in the Arkona Basin.

6.4 Inferred ΔR

When discussing the inferred ΔR, it is important to note that the benthic foraminifera we have dated are only able to exist in oxic conditions, while the Gotland Deep location from where we have retrieved our cores is prone to hypoxic conditions. As such, the occurrence of foraminifera is likely related to the inflow of oxic North Sea water at our study location, which allows a time window of favourable conditions for the establishment of a benthic foraminiferal community. After depletion of oxygen and/or lowered salinity of the inflow water mass, conditions once again become unfavourable for benthic foraminifera. Unfavourable conditions are typically recorded in the sediment by the preservation of laminated sediment with high LOI values. We have therefore not been able to make a ΔR estimate for intervals with higher LOI values, due to lack of significant numbers of foraminifera (Figure 2). The ΔR values are, therefore, most likely to reflect favourable conditions just after an inflow of oxic saline water, water which has been significantly altered due to entrainment with the shallower outflowing mass of brackish water. For example, present day inflowing saline water at the Öresund strait has a salinity in excess of 30, which is reduced in salinity to between 11 and 13.5 (SMHI, 2011) when it reaches the Gotland Deep. This entrainment is also likely to affect the ΔR value of the inflow water in a similar manner, as the radiocarbon content of the two water masses becomes mixed.

We note a general trend of decreasing ΔR values upwards in the core (Figure 9B), reflecting an increasing dominance of younger waters. It is proposed that this trend is due to a gradual change in hydrographic conditions. During the Littorina maximum (approx 7.5 ka ago), exchange with the open sea at the Öresund and the Danish Belts was greater than now and the Baltic proper was thought to be 6-8 units higher in salinity than now (Widerlund & Andersson, 2011), and some 47% greater in water volume (Meyer and Harff, 2005). Post-glacial isostatic rebound continued gradually throughout the Holocene and water exchange between the Baltic and the Kattegat/Skagerrak became reduced. The decrease in the influence of marine waters caused the salinity of the Baltic Sea to decrease to present day levels. We hypothesise that the trend towards younger ΔR values seen in Figures 9B and 10B is due to a decreasing influence of Kattegat/Skagerrak water through time, caused by decreasing exchange with the open sea and consequently more mixing and entrainment with the outflowing fresher water. This hypothesis for the decreasing ΔR values also implies that the outflowing brackish water mass must have a lower reservoir age than the inflowing saline water mass and, consequently, any hard-water effect present at our Gotland Deep study location in the open Baltic Sea must therefore be lesser in age than the reservoir age of the inflowing saline water. ^{14}C analysis of 20th century pre-bomb seaweeds of known ages in the shallow Baltic Sea (i.e. the fresher outflow water mass) near the south Swedish coast of Blekinge yielded comparatively young ΔR values of between -30 and -130 (Östlund and Engstrand, 1963; Engstrand, 1965; Olsson, 1980). This is less than the ΔR value of 200 for the inflow source water from the deeper water mass at the open sea in the Skaggerak, based on ^{137}Cs and ^{210}Pb age models (M. Moros, unpublished data). This difference in reported ΔR between the two locations supports our hypothesis of the shallow outflowing water being of younger age than the deeper inflowing water.

Generally we can say, when there is an absence of a significant hard-water effect or an input of older particulate organic matter, that a correlation between ΔR and salinity can be expected. Such an ideal correlation would be similar to the $\delta^{18}O$ vs. salinity and deuterium vs. salinity correlations found in modern Baltic Sea waters (Ehhalt, 1969; Fröhlich et al., 1988). However, more studies in other locations with different hydrographic conditions are required to quantify such a ΔR vs salinity correlation.

In addition to hydrographic conditions, some of the trend we note in ΔR values could also be caused by changes in the reservoir age of the two source waters themselves, i.e. the open sea at the Skagerrak and the river runoff water from the Baltic catchment

area. Additional research into temporal reservoir age changes for these two water bodies is also required.

7. Conclusion

It has been shown, by stacking the Littorina stage sediments of two PSV records from the Gotland Deep, that discernable PSV features can be recognised, whereby ages can be transferred to equivalent features present in the FENNOSTACK regional master curve (Snowball et al., 2007). For the Littorina stage sediments, PSV data was found to be most robust in burrow-mottled sediment and less robust in thinly laminated sediment. Using the methods employed in this study, it was not possible to ascertain continuous, useful PSV data from the deeper, Ancylus stage sediments due to the presence of an iron sulphide (most likely authigenic greigite), which complicates the interpretation of palaeomagnetic data due to the chemical remanent magnetisation that it acquires and its ability to acquire a strong gyroremanent magnetisation during alternating field demagnetisation.

The amplitude and trend of a declination swing encountered in Baltic Ice Lake stage sediments are similar to one found in palaeomagnetic studies of lakes in southern and central Sweden (Björck and Sandgren, 1986; Björck et al., 1987; Ising, 2001), whereby the chronology in those studies agrees with our stratigraphic intepretation. This agreement, coupled with the steady NRM signal encountered in the Baltic Ice Lake stage sediments, suggests that there is great potential for further palaeomagnetic studies of Baltic Ice Lake stage sediments in the central Baltic basin, which can be expected to further increase in temporal resolution downcore as the varved sediments become more proximal.

Despite very small sample sizes, state-of-the-art ^{14}C analysis has been used to carry out radiocarbon dating on foraminifera preserved in Baltic Sea sediments, which avoids the complications associated with dating bulk sediment. While the uncertainties inherent in our study make it difficult to make absolute estimates of ΔR downcore, comparison with a PSV & Pb depositional age model shows a trend of decreasing ΔR values from 7 ka ago to 1 ka ago. Furthermore, we also hypothesise that the reservoir age can change on a spatial basis, depending on the proximity of a study site to sources of river runoff or saline inflow. Many past studies of the Baltic Sea often assumed a single, constant value in the range of 250-400 years as a reservoir age correction when constructing radiocarbon age models. We strongly advise that reservoir ages in the Baltic Sea, as well as in other semi-enclosed brackish water basins, should be assessed on a local, study-by-study basis whereby temporal changes are also considered. Finally, one must also consider the type of fossil taxa being dated and the type of environment in which they thrive.

Acknowledgements

This research is part of the Inflow project (coordinated by A. Kotilainen, GTK Finland) and has received funding from the European Community's Seventh Framework Programme (FP/2007-2013) under grant agreement n° 217246 made with BONUS, the joint Baltic Sea research and development programme. R. Muscheler was funded by the Royal Swedish Academy of Sciences through a grant by the Knut and Alice Wallenberg Foundation. Radiocarbon dates have been funded in part by the Royal Physiographical Society of Lund. Editor C. Hillaire-Marcel (UQAM), reviewer J. Olsen (Queen's Belfast) and three anonymous reviewers contributed to significant improvements of this manuscript. A. Nilsson (Lund Univ.) is thanked for helping with the analysis of palaeomagnetic data. M. Reinholdsson (Lund Univ.) is thanked for help with magnetic units. S. Björck (Lund Univ.) is thanked for help with Baltic Sea stage intepretation. F. Adolphi (Lund Univ.) is thanked for discussions regarding ^{14}C dating. M. West (Durham Univ.) and L. Zillén (Lund Univ./SGU) are thanked for their helpful advice regarding Pb analyses. R. Endler (IOW) and A. Kotilainen are thanked for providing acoustic profile data. H. Filipsson (Lund Univ.) is thanked for discussions regarding foraminifera. All persons who helped with on-board core retrieval and palaeomagnetic subsampling, of which there are too many to name here, are greatly thanked for their invaluable assistance.

References

Bindler, R., Renberg, I., Rydberg, J., Andrén, T., 2009. Widespread waterborne pollution in central Swedish lakes and the Baltic Sea from pre-industrial mining and metallurgy. Environmental Pollution 157, 2132-2141.

Björck, S., 1995. A review of the history of the Baltic Sea, 13.0-8.0 ka BP. Quaternary International 27, 19-40.

Björck, S., Sandgren, P., 1986. A 2000 year geomagnetic record from two late Weichselian sequences in southeast Sweden. Geologiska foereningens i Stockholm foerhandlingar 108, 21-29.

Björck, S., Sandgren, P., Holmquist, B., 1987. A magnetostratigraphic comparison between ^{14}C years and varve years during the Late Weichselian, indicating significant differences between the time-scales. J. Quaternary Sci. 2, 133-140.

Brännvall, M.-L., Bindler, R., Emteryd, O., Renberg,

I., 2001. Four thousand years of atmospheric lead pollution in northern Europe: a summary from Swedish lake sediments. Journal of Paleolimnology 25, 421-435.

Bronk Ramsey, C., 2008. Deposition models for chronological records. Quaternary Science Reviews 27, 42-60.

Bronk Ramsey, C., 2009. Bayesian analysis of radiocarbon dates. Radiocarbon 51, 337-360.

Christiansen, C., Kunzendorf, H., Emeis, K.-C., Endler, R., Stuck, U., Neumann, T., Sivkov, V., 2002. Temporal and spatial sedimentation rate variabilities in the eastern Gotland Basin, the Baltic Sea. Boreas 31, 65-74.

Conley, D.J., Humborg, C., Rahm, L., Savchuk, O.P., Wulff, F., 2002. Hypoxia in the Baltic Sea and Basin-Scale Changes in Phosphorus Biogeochemistry. Environmental Science & Technology 36, 5315-5320.

Dergachev, V.A., Raspopov, O.M., Van Geel, B., Zaitseva, G.I., 2004. The "Sterno-Eutrussia" geomagnetic excursion around 2700 BP and changes of solar activity, cosmic ray intensity, and climate. Radiocarbon 46, 661-681.

Ehhalt, D.H., 1969. On the deuterium-salinity relationship in the Baltic Sea. Tellus 21, 429-435.

Engstrand, L., 1965. Stockholm natural radiocarbon measurements VI. Radiocarbon 7, 257-290.

Fröhlich, K., Grabczak, J., Rozanski, K., 1988. Deuterium and oxygen-18 in the baltic sea. Chemical Geology: Isotope Geoscience section 72, 77-83.

Van Geel, B., Mook, W., 1989. High-resolution ^{14}C dating of organic deposits using natural atmospheric ^{14}C variations. Radiocarbon 31, 151-155.

Hedenström, A., Possnert, G., 2001. Reservoir ages in Baltic Sea sediment—a case study of an isolation sequence from the Litorina Sea stage. Quaternary Science Reviews 20, 1779-1785.

Hughen, K.A., Baillie, M.G.L., Bard, E., Beck, J.W., Bertrand, C.J.H., Blackwell, P.G., Buck, C.E., Burr, G.S., Cutler, K.B., Damon, P.E., Edwards, R.L., Fairbanks, R.G., Friedrich, M., Guilderson, T.P., Kromer, B., McCormac, G., Manning, S., Bronk Ramsey, C., Reimer, P.J., Reimer, R.W., Remmele, S., Southon, J.R., Stuiver, M., Talamo, S., Taylor, F.W., Van der Plicht, J., Weyhenmeyer, C.E., 2004. Marine04 marine radiocarbon age calibration, 0-26 cal kyr BP. Radiocarbon 46, 1059-1086.

IOC, IHO, BODC, 2003. Centenary Edition of the GEBCO Digital Atlas. British Oceanographic Data Centre, Liverpool.

Ising, J., 2001. Late Weichselian pollen stratigraphy, clay varve chronology and palaeomagnetic secular variations in Lake Bolmen, Småland, south Sweden. Boreas 20, 189-205.

Kilian, M.R., Van der Plicht, J., Van Geel, B., 1995. Dating raised bogs: New aspects of AMS ^{14}C wiggle matching, a reservoir effect and climatic change. Quaternary Science Reviews 14, 959-966.

Kirschvink, J.L., 1980. The least-squares line and plane and the analysis of palaeomagnetic data. Geophysical Journal of the Royal Astronomical Society 62, 699-718.

Kochegura, V.V., 1992. Use the Paleomagnetic Methods for Geological Mapping of Sea Shelf (In Russian). VSEGEI, St. Petersburg.

Kortekaas, M., 2007. Post-glacial history of sea-level and environmental change in the southern Baltic Sea. PhD thesis (Lundqua thesis 57). Lund University. Available at: http://www.geol.lu.se/kvg/avhandlingar/mk_kappa.pdf

Kortekaas, M., Murray, A.S., Sandgren, P., Björck, S., 2007. OSL chronology for a sediment core from the southern Baltic Sea: A continuous sedimentation record since deglaciation. Quaternary Geochronology 2, 95-101.

Kotilainen, A.T., Saarinen, T., Winterhalter, B., 2000. High-resolution paleomagnetic dating of sediments deposited in the central Baltic Sea during the last 3000 years. Marine Geology 166, 51-64.

Meyer, M., Harff, J., 2005. Modelling Palaeo Coastline Changes of the Baltic Sea. Journal of Coastal Research 21, 598-609.

Murray, J., 2006. Ecology and Applications of Benthic Foraminifera, 1st ed. Cambridge University Press, Cambridge.

Nöel, M., Tarling, D.H., 1975. The Laschamp geomagnetic "event". Nature 253, 705-707.

Olsson, I.U., 1980. Content of C-14 in marine mammals from northern Europe. Radiocarbon 22, 662-675.

Östlund, H., Engstrand, L., 1963. Stockholm Radiocarbon Measurement V. Radiocarbon 5, 203-227.

Van der Plicht, J., 2005. Radiocarbon, the Calibration Curve and Scythian Chronology, in: Impact of the Environment on Human Migration in Eurasia, NATO Science Series: IV: Earth and Environmental Sciences. Springer Netherlands, pp. 45-61.

Potter, D.K., Stephenson, A., 1986. The detection of fine particles of magnetite using anhysteretic and rotational remanent magnetizations. Geophysical Journal of the Royal Astronomical Society 87, 569-582.

Reimer, P.J., Baillie, M.G.L., Bard, E., Bayliss, A., Beck, J.W., Blackwell, P.G., Bronk Ramsey, C., Buck, C.E., Burr, G.S., Edwards, R.L., Friedrich, M., Grootes, P.M., Guilderson, T.P., Hajdas, I., Heaton, T.J., Hogg, A.G., Hughen, K.A., Kaiser, K.F., Kromer, B., McCormac, F.G., Manning, S.W., Reimer, R.W., Richards, D.A., Southon, J.R., Talamo, S., Turney, C.S.M., Van der Plicht, J., Weyhenmeye, C.E., 2009. IntCal09 and Marine09 radiocarbon age calibration curves, 0–50,000 years cal BP. Radiocarbon 51, 1111-1150.

Renberg, I., Bindler, R., Brännvall, M.-L., 2001. Using the historical atmospheric lead-deposition record as a chronological marker in sediment deposits in Europe. The Holocene 11, 511-516.

Rößler, D., Moros, M., Lemke, W., 2011. The Littorina transgression in the southwestern Baltic Sea: new insights based on proxy methods and radiocarbon dating of sediment cores. Boreas 40, 231-241.

Ruff, M., Szidat, S., Gäggeler, H.W., Suter, M., Synal, H.-A., Wacker, L., 2010. Gaseous radiocarbon measurements of small samples. Nuclear Instruments and Methods in Physics Research Section B: Beam Interactions with Materials and Atoms 268, 790-794.

SMHI, 2011. Oceanographic data for station BY15 (Gotland Deep). Sveriges Oceanografiska Data Center, SMHI, Norrköping.

Snowball, I., 1999. Electromagnetic units and their use in environmental magnetic studies., in: Environmental Magnetism: a Practical Guide.

Technical Guide No. 6. Quaternary Research Association, London, pp. 90-98.
Snowball, I., Torii, M., 1999. Incidence and significance of ferrimagnetic iron sulphides in Quaternary studies., in: B.A. Maher and R. Thompson (eds) Quaternary Climate, Environments and Magnetism. Cambridge University Press, pp. 199-230.
Snowball, I., Zillén, L., Ojala, A., Saarinen, T., Sandgren, P., 2007. FENNOSTACK and FENNORPIS: Varve dated Holocene palaeomagnetic secular variation and relative palaeointensity stacks for Fennoscandia. Earth and Planetary Science Letters 255, 106-116.
Snowball, I.F., 1997. The detection of single-domain greigite (Fe_3S_4) using rotational remanent magnetization (RRM) and the effective gyro field (Bg): mineral magnetic and palaeomagnetic applications. Geophysical Journal International 130, 704-716.
Sohlenius, G., 1996. Mineral magnetic properties of Late Weichselian-Holocene sediments from the northwestern Baltic Proper. Boreas 25, 79-88.
Sohlenius, G., Emeis, K.-C., Andrén, E., Andrén, T., Kohly, A., 2001. Development of anoxia during the Holocene fresh–brackish water transition in the Baltic Sea. Marine Geology 177, 221-242.
Stephenson, A., Snowball, I.F., 2001. A large gyromagnetic effect in greigite. Geophysical Journal International 145, 570-575.
Stuiver, M., Braziunas, T.F., 1993. Modeling atmospheric ^{14}C influences and ^{14}C ages of marine samples to 10,000 BC. Radiocarbon 35, 137-189.
Turner, G.M., Thompson, R., 1981. Lake sediment record of the geomagnetic secular variation in Britain during Holocene times. Geophysical Journal of the Royal Astronomical Society 65, 703-725.
Virtasalo, J.J., Leipe, T., Moros, M., Kotilainen, A.T., 2012a. Physicochemical and biological influences on sedimentary-fabric formation in a salinity and oxygen-restricted semi-enclosed sea: Gotland Deep, Baltic Sea. Sedimentology 58, 352-375.
Virtasalo, J.J., Bonsdorff, E., Moros, M., Kabel, K., Kotilainen, A.T., Ryabchuk, D., Kallonen, A., Hämäläinen, K., 2012b. Ichnological trends along an open-water transect across a large marginal-marine epicontinental basin, the modern Baltic Sea. Sedimentary Geology, 241, 40-51.
Wacker, L., Lippold, J., Molnár, M., Schulz, H., submitted. Towards single-foraminifera-dating with a gas ion source. Nuclear Instruments and Methods B.
Widerlund, A., Andersson, P.S., 2011. Late Holocene freshening of the Baltic Sea derived from high-resolution strontium isotope analyses of mollusk shells. Geology 39, 187 -190.
Winterhalter, B., Flodén, T., Ignatius, H., Axberg, S., Niemistö, S., 1981. Geology of the Baltic Sea, in: The Baltic Sea (ed. Voipio, A.). Elsevier, Amsterdam, pp. 1-121.
Zillén, L., Conley, D.J., Andrén, T., Andrén, E., Björck, S., 2008. Past occurrences of hypoxia in the Baltic Sea and the role of climate variability, environmental change and human impact. Earth-Science Reviews 91, 77-92.
Zillén, L., Lenz, C., Jilbert, T., 2012. Stable lead (Pb) isotopes and concentrations - a useful independent dating tool for Baltic Sea sediments. Quaternary